LUND UNIVERSITY

Satellite Monitoring of Railways using Interferometric Synthetic Aperture Radar (InSAR)

Palmqvist, Carl-William; Ochsner, Michelle; Jamali, Sadegh; Hashemi, Hossein; Åmerbilly, Kara; Nilfouroushan , Faramarz ; Bagherbandi , Mohammad; Karim, Ramin; Kour, Ravdeep; Åldstedt, Rolf; Norrbin, Per

2021

Document Version:
Publisher's PDF, also known as Version of record

Link to publication

Citation for published version (APA):
Palmqvist, C.-W., Ochsner, M., Jamali, S., Hashemi, H., Åmerbilly, K., Nilfouroushan , F., Bagherbandi , M., Karim, R., Kour, R., Åldstedt, R., & Norrbin, P. (2021). *Satellite Monitoring of Railways using Interferometric Synthetic Aperture Radar (InSAR)*. Lund University.

Total number of authors:
11

General rights
Unless other specific re-use rights are stated the following general rights apply:
Copyright and moral rights for the publications made accessible in the public portal are retained by the authors and/or other copyright owners and it is a condition of accessing publications that users recognise and abide by the legal requirements associated with these rights.
• Users may download and print one copy of any publication from the public portal for the purpose of private study or research.
• You may not further distribute the material or use it for any profit-making activity or commercial gain
• You may freely distribute the URL identifying the publication in the public portal

Read more about Creative commons licenses: https://creativecommons.org/licenses/

Take down policy
If you believe that this document breaches copyright please contact us providing details, and we will remove access to the work immediately and investigate your claim.

LUND UNIVERSITY

PO Box 117
221 00 Lund
+46 46-222 00 00

LUND UNIVERSITY | LTH FACULTY OF ENGINEERING

Satellite Monitoring of Railways using Interferometric Synthetic Aperture Radar (InSAR)

Submitted To: Trafikverket

2021-19-11

Carl-William Palmqvist (LU)

Michelle Ochsner (LU)

Sadegh Jamali (LU)

Kara Åmerbilly (LU)

Hossein Hashemi (LU)

Faramarz Nilfouroushan (HiG)

Mohammad Bagherbandi (HiG)

Ramin Karim (LTU)

Ravdeep Kour (LTU)

Rolf Åldstedt (SWECO)

Per Norrbin (SWECO)

This project was financed by Trafikverket (The Swedish Transport Administration), grant 7194

Table of Contents

Abstract

There is over 15,600 km of track in the Swedish railroad network. This network is vital for the transportation of people and goods across the country. It is important that this network is monitored and maintained to ensure good function and safety. A tool for monitoring and measuring ground deformation over a large area remotely with high frequency and accuracy was developed in recent decades. This tool is known as Interferometric Synthetic Aperture Radar (InSAR), and is used by researchers, geo-technicians, and engineers.

The purpose of this study has been to evaluate the use and feasibility of the InSAR technique for track condition monitoring and compare it to conventional track condition monitoring techniques. Malmbanan, which is primarily used to transport iron-ore from mines in Sweden to the ports of Luleå, Sweden and Narvik, Norway, is used as a case study for this project; specifically, the section between Kiruna and Riksgränsen. Coordinate matching of measurements from the provided Persistent Scatterer Interferometry (PSI) InSAR data and Optram data from survey trains were performed. Then measured changes over different time spans within the two systems were overlapped and classified with different thresholds to see if there is correlation between the two systems. An extensive literature review was also conducted in order to gain an understanding of InSAR technologies and uses.

The literature review showed that there is a large potential and a quickly growing number of applications of InSAR to monitor railways and other types of infrastructure, and that the tools and algorithms for this are being improved. The case study, on the other hand, shows that it can be difficult to directly compare measurement series from different tools, each working on different resolutions in terms of both time and space. InSAR is thus not about to replace techniques such as those behind Optram (using measurement trains). Instead, the approaches offer complementary perspectives, each highlighting different types of issues.

We find that InSAR offers a good way to identify locations with settlements or other types of ground motions. Especially transition zones between settlements and more stable ground can be challenging from a maintenance point of view and can clearly be identified and monitored using InSAR. With the rollout of national InSAR-data, and the large increase in data accessibility, we see a considerable potential for future studies that apply the technique to the railway area.

Sammanfattning

Det finns över 15 600 km spår i det svenska järnvägsnätet. Detta nätverk är avgörande för transport av människor och varor över hela landet. Det är viktigt att detta nätverk övervakas och underhålls för att säkerställa god funktion och säkerhet. Under de senaste decennierna har ett verktyg för att övervaka och mäta markdeformation över ett stort område på distans med hög frekvens och noggrannhet utvecklats. Detta verktyg kallas för InSAR (Interferometric Synthetic Aperture Radar) och används av forskare, geotekniker och ingenjörer.

Syftet med detta projekt har varit att utvärdera möjligheten att använda InSAR-teknik för att övervaka järnvägens tillstånd, och jämföra den med andra befintliga tekniker. Dels har en omfattande litteraturgenomgång genomförts för att få en förståelse för hur InSAR fungerar och använts runtom i världen. Dels har en fallstudie genomförts på en del av Malmbanan. Mellan Kiruna och Riksgränsen har vi matchat mätserier från InSAR och Optram (från mättåg) med varandra, för att se i vilken omfattning de mäter och identifierar samma förändringar.

Litteraturstudien visar att det finns en stor potential och ett snabbt växande antal tillämpningar av InSAR för att övervaka järnväg och annan typ av infrastruktur, och att metoderna för detta snabbt håller på att utvecklas. Fallstudien visar å andra sidan att det är komplicerat att direkt jämföra mätserier från olika verktyg, som använder sig av olika upplösningar i både tid och rum. InSAR kommer därför inte över en överskådlig framtid att ersätta tekniker som de bakom Optram vad gäller mätning av spårgeometri, utan det handlar i stället om kompletterande tekniker, som utifrån sina olika perspektiv belyser olika typer av utmaningar.

Vi visar att InSAR med fördel kan användas för att identifiera platser där det finns sättning eller andra typer av markrörelser. Särskilt gränszoner kan vara känsliga ur en underhållssynpunkt, dessa kan tydligt identifieras och övervakas med hjälp av InSAR. Med utrullning av nationella InSAR-data, och den därmed kraftigt förbättrade datatillgången, ser vi en stor potential för vidare studier som använder tekniken inom järnvägsområdet.

1. Introduction

Land surface vertical displacements is an emerging issue that has large potential to jeopardise sustainability worldwide. Natural and anthropogenic activities may result in land deformation and compaction of compressible fine-grained sub-surface soils with the possible consequence of damaging infrastructures such as railroads, buildings, and constructions. During the last few decades, anthropogenic activities have been dramatically increased due to population growth and industrialisation, and land and water resources are being further stressed by new urban, agricultural, and industrial development. The stress is partly due to population increase but also due to expected climate change. These activities have resulted in displacement of land surface due to extraction of groundwater for drinking, agricultural, and industry as well as mining, which consequently impact the sustainability of natural and manmade systems in both short- and long-runs.

Regarding railways specifically, railways are operating at faster speeds, with higher axle loads while ridership continues to increase (Yang, Schmid, & Roberts, 2015). Track subsidence, which refers to the permanent settlement of both the subgrade and track, and the effects of climate change are also shown to play a factor in railway punctuality and maintenance costs (Kellermann et al., 2015; Yang, 2015; Yang, Schmid, & Roberts, 2015). These factors lead towards the importance of railway monitoring to ensure railway operations run smoothly, safely, and with minimal delays (Liu et al., 2014; Misnevs, Melikyan, & Bazards, 2015).

Constant monitoring decreases the life cycle costs of a rail due to the reduction of maintenance work required (Yang, 2015). Conventional monitoring of railways involves in-situ methods, such as leveling or deployment of survey trains. These methods are often labour intensive, expensive, and time consuming, and therefore are only applied on a limited scale in time and space. Additionally, some in-situ monitoring methods cannot be performed while the track is in use (Chang et al., 2014).

Interferometric Synthetic Aperture Radar techniques (InSAR) is a remote sensing technique that can measure the ground surface deformation caused by factors such as, mining activities, the pumping of groundwater, tectonic plate movement, natural compression of the soil layer, peatland evolution, and permafrost activity with sub-centimeter accuracy. It can also be applied to complement the limits of conventional methods, detect changes in elevation on a millimeter scale (Chang et al., 2014), and compared to conventional techniques, it can cover large areas while operating remotely. InSAR can cost effectively monitor railways without the need for specialised equipment or in-situ presence (Tosti et al., 2020). Prior research has proven InSAR to be an available tool for monitoring topographic elevation and ground deformation. InSAR was first used in 1989 to measure ground deformation (Gabriel, 1989) and since then new methods and applications have been discovered. The potential of InSAR in the realm of transportation infrastructure monitoring is relatively new and has yet to be sufficiently explored (Tosti et al., 2020). However, there is research on other InSAR techniques, such as permafrost, landslide, or temperature monitoring which can be applied to monitoring railways. Therefore, InSAR can be used in several different applications and can be very useful in the realm of railway planning and maintenance.

InSAR may help reduce the need for costly in-situ monitoring and maintenance methods of track geometry and displacements which also consumes network capacity. InSAR can also provide data for improved degradation models; and improve the identification and monitoring of potentially hazardous areas, in terms of risks such as rail buckling, flooding, and landslides. Finally, InSAR provides considerable benefits in generating detailed and updated maps of the networks, with the precise location of various components.

There are two main aims of this study. The first is to analyse structural deformation and track displacement using Sentinel-1 SAR data and compare it to Optram data currently used by Trafikverket. The second is to assess the feasibility of developing satellite-based monitoring

and maintenance system for the entire Swedish railway network, including track displacements as well as risks of floods and landslides near railways. The project is one step towards digitising railways for a sustainable future.

2. Climate Change Concerns

Climate change has been an issue of concern over the last decades and the need for adaptation and resiliency in societies and systems is an increasing topic of discussion (Lindgren, Jonsson, & Carlsson-Kanyama, 2009). The IPCC (2014a) suggests that it is becoming more evident that the alarming increase in mean annual temperature is a result of climate change. Furthermore, it is understood that the continuation of greenhouse gas emissions (GHG) will cause not only further warming but long-lasting changes in our climate system leading to irreversible impacts for all ecosystems and people. With a drastic reduction in GHG emissions and more adaptation strategies, the risks of climate change can be limited.

The IPCC (2014b) states that the average temperature in Europe continues to increase, with rates of warming being the most prominent in the high latitudes of Northern Europe. Since the 1980s, Scandinavia has experienced the strongest warming, especially during the winter months. Annual precipitation rates have increased in Northern Europe, with projections leaning towards more rain than snow in mountainous regions. Specifically, above the Arctic Circle, physical infrastructure stability is reliant on climate conditions, sea ice conditions, permafrost, and snow. Although much of the infrastructure is built with weather conditions in mind, the rapidly changing climate has left infrastructure more vulnerable and inadequate to respond to natural disasters and environmental emergencies. The regions safety, environmental integrity, and security are highly dependent on transportation infrastructure as the main method for transporting goods and services to these remote areas. Therefore, it is essential to create a transportation sector that is resilient to climate change and able to quickly adapt.

2.1. Climate Change Within the Transportation Sector

One sector that will become more affected by the risks of climate change is the transportation sector, in particular railway infrastructure. Railways will be more susceptible to major events such as flooding, severe storms, landslides, and track buckling in the future in relation to climate change. Transportation infrastructure has a long-life span and great economic value, therefore its resilience and preparedness to the impact of climate change is crucial (European Commission, 2013). Nolte, Kamburow, and Rupp (2011) discuss the concept of integral risk management which comprises four phases: inventory and identification of risks, risk analysis, risk evaluation, and risk management. This integrated strategy follows the guiding principle of the three Rs: readiness, resilience, and recovery. Overall, the report discusses and analyses various case studies to highlight the importance of risk assessment and monitoring in order to provide better risk management strategies.

Generally, infrastructure is constructed in a manner that is resilient to past weather conditions, and therefore there should be more of a focus on how to make infrastructure more resilient for the future (European Commission, 2013). Additionally, literature reveals there is a great emphasis on involving key stakeholders and raising awareness during decision making as the stakeholders' knowledge and adaptive capacity are key to achieving the right results (European Commission, 2013). The impacts of climate change are not just solely a function of weather events, but also of a network's vulnerability (Baker et al., 2009). Typically, railways are considered to be more vulnerable compared to road infrastructure due to lack of excess capacity, single line tracks, and limited rerouting options (Mattsson & Jenelius, 2015). Additionally, less focus is dedicated to rail and waterborne transportation in relation to climate change research publications compared to road or air (Aparicio et al., 2013). Therefore, it is evident that adaptation and resilience are key factors in achieving long-term successful railway systems.

Kellermann et al. (2016) analysed the possible impacts of climate change on the frequencies of critical meteorological conditions (CMCs) between 1961-1990 and 2011-2040. The study

was conducted in Austria where railways, due to the mountainous environment, typically follow floodplains, where they are more prone to flooding and other alpine hazards (e.g., rockfalls, avalanches, or landslides). Due to climate change it is expected that the railways will be more at risk. In recent years, natural hazard and risk management has shifted from technological approaches to a more integrated risk management strategy. The Austrian Federal Railways (ÖBB) is an example of a rail operator which puts an emphasis on non-structural, precautionary risk mitigation measures such as weather warning and forecasting systems. This study highlights the importance of proper climate and weather preparation and the importance of a more integrated risk management strategy.

3. Track Geometry

In the past, railway maintenance was typically planned based on the experience and knowledge of the infrastructure owner with the main goal geared towards providing a high level of safety with little concern towards economic and operational optimisation issues (Khouy et al., 2014a). Today, there is more focus on cost-effective maintenance limits in order to optimise operation and maintenance due to the deregulated competitive environment and budget limits; however, the goal should be more geared towards making operation and maintenance cost-effective while meeting high safety standards (Khouy et al., 2014a). As railway speed and axle limits increase it is important to inspect and maintain tracks regularly in order to maintain the safety and reliability of the railway (Kim et al., 2009). Track irregularities can affect the safety of a train, its running behaviour, and the comfort of passengers (Kim et al., 2009). When trains pass the tracks, this causes cyclic movements of the unbound particles which results in vertical deformations of the track reducing track geometry quality, safety, and comfort (Sol-Sánchez & D'Angelo, 2017).

Majority of railway maintenance is concerned with track geometry, where preventative condition-based maintenance is used to control the degradation of the track and restore track geometry conditions to an acceptable state (Soleimanmeigouni et al., 2020). Geotechnical defects such as poor drainage of the subgrade and initial compaction of the ballast contribute to subsidence and changes in the track geometry (Yang, 2015). As mentioned, a major disadvantage to many traditional surveying methods such as total stations, precise levelling, and track-recording cars is that they take a significant amount of time and are typically highly expensive (Liu et al., 2014). Because railways are long linear constructions that subside continuously over time, levelling and GPS approaches have limitations in monitoring railway subsidence (Yang, 2015).

3.1. Monitoring of Track Geometry

The railway system is a complex technical system which consists of railway infrastructure and rolling stock. Railway track or railroad is a part of railway infrastructure consisting of parallel lines of rails with their sleepers, fittings and fastenings, ballast, etc., which enables trains to move for the transportation of passengers and freight. From time to time these tracks need regular maintenance due to constant movement of heavy and high-speed trains. Due to the vibrations, climatic conditions, and impact of high-speed trains, the packing under the sleepers becomes loose, track geometry gets disturbed, and there is heavy wear and tear of the track and its components. Track geometry refers to the position of each rail or the track centre line in three-dimensional space (Arema, 2013). Track geometry is a key aspect of safety and ride quality. According to Xu et al. (2013), track deterioration depends on factors such as formation condition, in specific in relation to the effectiveness of the drainage system, ballast quality, traffic loading, type of track construction, dimension of track components, curvature, and quality of materials. Thus, regular track maintenance will improve its lifetime, reduces operational costs and fuel consumption, provide safe and smooth running of trains without any unnecessary failure.

Railway track condition data for the Swedish railways are collected by measurement wagons that regularly are pulled along the track system in speeds up to 200 km/h (Bergquist & Söderholm, 2016). Each section of the Swedish track system is measured up to six times per year (Bergquist & Söderholm, 2016). The main geometry parameters used to assess track quality and plan maintenance activities are gauge, alignment, longitudinal level, cant, and twist. The track geometry parameters are described by a relative rectangular co-ordinate system centred to the track (SS-EN 13848-1: 2004+A1, 2008) in Table 1.

Table 1. Track geometry parameters used to assess track quality and plan maintenance (SS-EN 13848-1: 2004+A1, 2008)

Parameter description	Visual description
***Track gauge*:** This parameter is the distance G between two adjacent rails from point P at distance $z_{p=}14$ mm below the running surface (SS-EN 13848-1: 2004+A1, 2008). The nominal track gauge for a standard track is 1435 mm (SS-EN 13848-1: 2004+A1, 2008).	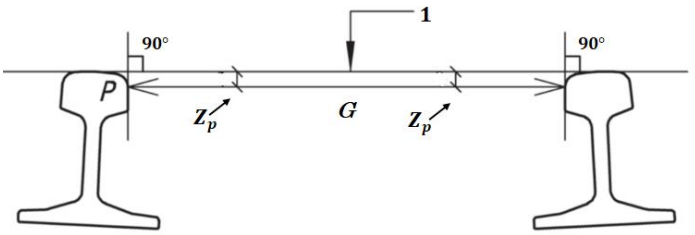
Alignment: This parameter is defined as the horizontal deviation (y_p) of consecutive positions of point P on the left or the right rail from the mean horizontal position (the reference line) (SS-EN 13848-1: 2004+A1, 2008)	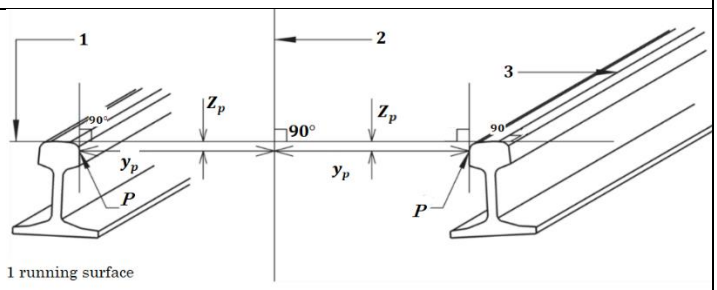
Longitudinal level/ Vertical profile: This parameter is defined as the vertical deviation ($z_{p'}$) of consecutive running table levels on the top of the left or right rail from the mean vertical position (the reference line) (SS-EN 13848-1: 2004+A1, 2008)	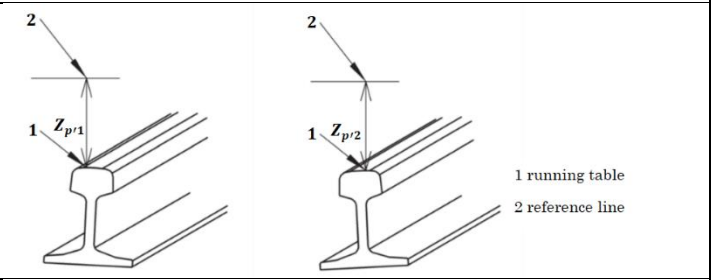
Cant: This parameter also called as cross level is defined as the difference in height of the adjacent running tables computed from the angle between the running surface and a horizontal reference plane (SS-EN 13848-1: 2004+A1, 2008)	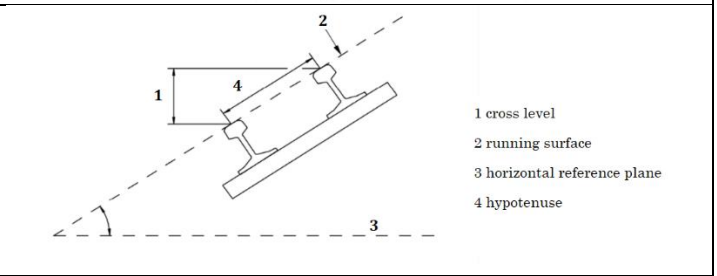
Twist: This parameter is the variation in actual track cross level over a defined length. It is calculated as an algebraic difference between two cross level values measured at positions located at a specified distance from each other.	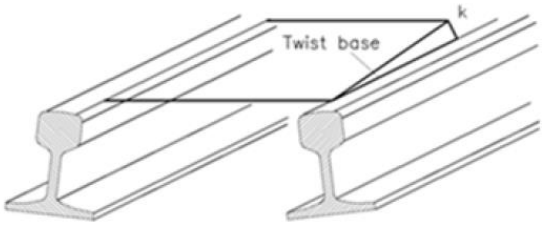

Because of the influence of dynamic track loads, the track geometry degrades and deviates from the designed vertical and horizontal alignments (Soleimanmeigouni, 2019). EN 13848-5 (2008) has specified three ranges of wavelengths (λ) to evaluate the track geometry. These are:

1. D1: 3 m < λ ≤ 25 m,
2. D2: 25 m < λ ≤ 70 m,
3. D3: 70 m < λ ≤ 150 m.

To consider the short wavelength defects, the lower bound of D1 must go down to 1 m. The running behaviour of the train is influenced by wavelengths and the amplitude of the track irregularities. Short wavelength defects become dangerous because their amplitude is high, therefore, more attention is needed for them (EN 13848–5, 2008).

The three indicators mainly used to represent the track geometry quality are (SS-EN 13848-1: 2004+A1, 2008):

1. Extreme values of isolated defects;
2. Standard deviation over a specified length, usually 200 m;
3. Mean value.

The standard deviation (SD) is the Track Quality Index (TQI) mostly used by European railway networks (EN 13848–5 2008). It is recommended to calculate SD for the left and the right rail separately. The SD is usually calculated for track sections with a length of 100 m or 200 m, but it can also be calculated for longer track sections, for example, sections with a length of 1 km. Commonly, the standard deviation is calculated for the vertical level and horizontal alignment irregularities in the wavelength range D1. It is also calculated for other parameters, including twist, gauge, and cant (EN 13848-6 2012). The SD is used to represent the variation of track geometry measurement data. A low standard deviation indicates that the geometry measurements are close to the mean and a high standard deviation indicates that the geometry measurements have a high variation around the mean value. It could be argued that a higher standard deviation reflects more irregularities in the track.

Three maintenance levels are defined to evaluate the severity of the track geometry deviation (SS-EN 13848-1: 2004+A1, 2008). All the five track geometry parameters must be prescribed through the indicators provided in Table 2 as a minimum requirement (EN 13848-1: 2004+A1, 2008).

Table 2. Maintenance levels to evaluate the severity of the track geometry deviation (Arasteh Khouy, 2013; Soleimanmeigouni, 2019; SS-EN 13848-1: 2004+A1, 2008).

Maintenance levels	Description
Intermediate Action Limit (IAL)	This is a safety limit; if the deviation exceeds this limit, there is a risk of derailment. The risk can be reduced by closing the line, reducing the speed, or correcting track geometry.
Intervention Limit (IL)	This is a corrective maintenance limit; if the deviation goes beyond this limit, corrective maintenance should be performed so that the immediate action limit will not be reached before the next inspection.
Alert Limit (AL)	This is a preventive maintenance limit; if the deviation exceeds this limit, the track geometry condition should be analysed and included in the regularly planned maintenance operations.

3.2. Optram

Optram (OPtimized TRAck Management) is the track geometry measurement database which has been used since 2007 by Banverket (the former Swedish Rail Administration) and Trafikverket (the Swedish Transport Administration) for the study of measurements performed on the track and overhead lines (Trafikverket, 2021a). The Optram database contains information about railway infrastructure together with information about when and where the

measurements were performed (Bergquist & Söderholm, 2016). This system visualises and graphically represents the track geometry measurements. Optram provides functionality for analysis and displays data trends. Inspections are carried out by measurement cars approximately four to six times a year depending upon the track characteristics for every 25 cm. There are two types of recording cars one STRIX and three IMV100 that are used to measure track geometry quality in Sweden (Lander & Petersson, 2012). They provide various measurements parameters related to track geometry measurements, and other related information such as location, type of track, and the presence of special objects. Figure 1 represents Optram Database Process that shows how this system is connected to other database systems.

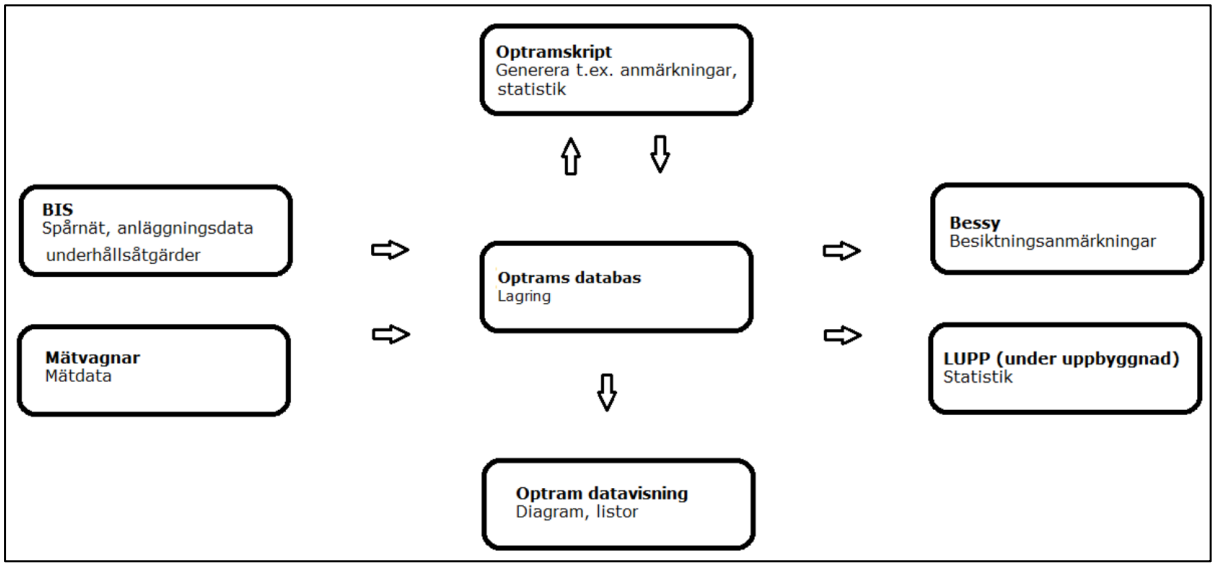

Figure 1. Optram Database Process (Trafikverket, 2020a)

In addition, other information such as Optram user manual, data documentation, and setting files in Optram are also provided by Trafikverket (Trafikverket, 2018; Trafikverket, 2020b. Following Table 3 shows list of all the measurement points stored in the Optram database:

Table 3. Optram Measurement Points

Sno.	OPTRAM Parameter Name
1	Samverkan rfh sidoläge (mm)
2	Kvalitetsklass (n/a)
3	Stationsområde (n/a)
4	Höjd kortvåg vänster (mm)
5	Höjd mellanvåg vänster (mm)
6	Höjd långvåg vänster (mm)
7	Höjd kortvåg höger (mm)
8	Ofiltrerad höjd H (mm)
9	Höjd mellanvåg höger (mm)
10	Ofiltrerad sida H (mm)
12	Höjd långvåg höger (mm)
13	Sido kortvåg vänster (mm)
14	Sido mellanvåg vänster (mm)
15	Sido långvåg vänster (mm)
16	Sido kortvåg höger (mm)
17	Sido mellanvåg höger (mm)
18	Sido långvåg höger (mm)
19	Spårvidd (mm)
20	Kurvatur (1/m)
21	Rälsförhöjning (mm)
22	Hastighet (km/h)
23	GPS-koordinater SWEREF 99 N (m)
24	GPS-koordinater SWEREF 99 E (m)
25	Sido kortvåg 1–15 m vänster (mm)
26	Sido kortvåg 1–15 m höger (mm)
27	Skevning 3m bas (mm)
28	Skevning 6m bas (mm)
29	Std höjd (mm)
30	Std rälsförhöjning (mm)
31	Std sida (mm)
32	Std samverkan (mm)
33	Q-tal
34	Spårviddsändring 10m (mm)
35	Spårvidd 100m medel (mm)
36	Rälsförhöjningens ojämnhet (mm)
37	Ofiltrerad höjd V (mm)
38	QS-tal (N/A)
39	Ofiltrerad sida V (mm)
40	SDH Höjd ENnorm (mm)
41	SDS Sida ENnorm (mm)
42	SDSAM samverkan (mm)

For this study, we used the following Optram parameters related to longitudinal level. A total of 24 sets of data was given for the Optram data, and each set contained about 40 different collected measurements; in Optram they are labelled as Höjd kortvåg vänster (mm), Höjd mellanvåg vänster (mm), Höjd långvåg vänster (mm), Höjd kortvåg höger (mm), Höjd

mellanvåg höger (mm), Höjd långvåg höger (mm), and SDSAM samverkan (Table 3). Optram measurements used for this study were from between 6 April 2015 – 26 June 2020.

4. Interferometric Synthetic Aperture Radar (InSAR) Background

Continuous monitoring is crucial in assessing infrastructure instabilities. This plays a pivotal role in urban development and in mitigating damages and disasters in different environmental and engineering components such as large-scale human-made linear features. Such features may include railways, tunnels, roads, and bridges. These objects can be monitored and analysed using terrestrial- and satellite-based geodetic methods, for example by high-precision levelling, total stations, laser scanning, Global Navigation Satellite System (GNSS), and the Synthetic Aperture Radar (SAR) images.

4.1. Active Radar

An active radar sensor generates its own source of light, unlike passive sensors which rely on an external light source, for instance the sun (Figure 2). In an active radar, the electromagnetic energy hits the Earth's surface scattering the energy, then some of this scatter returns to a broadcasting system. This is then registered and stored for further interpretation (Campbell & Wynne, 2011). The ability of an active radar sensor to be able to generate its own light enables it to operate day and night (Lillesand, Kiefer, & Chipman, 2014).

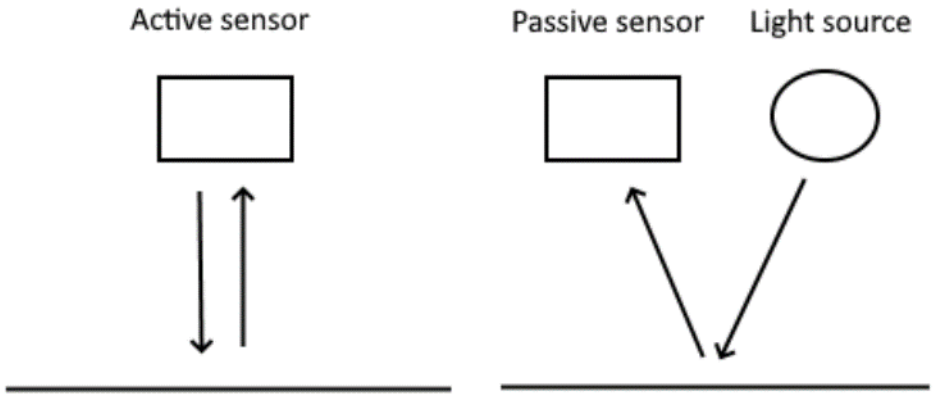

Figure 2. Depiction of an Active Sensor which Generates its Own Light Source vs. a Passive Sensor which is Dependent on an External Light Source (Åmerbilly, 2021)

The active radar emits energy as microwaves, which exist on the electromagnetic spectrum between the length of about 1 mm to 1 m. There are two properties that make microwaves beneficial over visible wavelengths. The first is that microwaves are able to operate under most weather conditions. The second property is that microwaves can penetrate through clouds, rain, haze, and smoke (Campbell & Wynne, 2011; Lillesand, Kiefer, & Chipman, 2014).

4.2. Synthetic Aperture Radar (SAR)

Synthetic Aperture (SAR) is a remote sensing technique used for both ocean and land observations. SAR sensors are active meaning they create their own source of illumination, emit artificial radiant energy, and measure that reflected energy (Fryksten, 2019). These sensors are typically mounted on moving platforms such as satellites and use movement to create a synthetic antenna which is longer than the physical antenna on the platform allowing for high resolution images (Fryksten, 2019).

When the transmitted microwaves reach the Earth's surface, they get reflected off the surface or off an object existing on the surface. The reflected microwaves are then received by the antenna as backscatter (Lillesand, Kiefer, & Chipman, 2014). The typical frequency for the pulses range between 100s to 1000s Hz for airborne and spaceborne systems. The area that can be illuminated varies from a few kilometres to 20 km for airborne systems and between 30 to 500 km for spaceborne systems (Moreira et al., 2013). A radar system that only uses one antenna for transmitting and receiving is called monostatic, whereas one that uses separate antennas for transmitting and receiving is called bistatic (Hanssen, 2002). Properties of the backscatter, such as amplitude and phase, depend on the physical and electrical properties of the imaged object (Ager, 2013). Until the 1950s imaging radars were referred to as side looking airborne radar (SLAR). Azimuth resolution is the smallest separation between two objects that can be detected by the radar. For example, a SLAR system with a 3 m antenna at a 5 km range has an azimuth resolution of 50 m (Moreira et al., 2013). This low resolution has been the main disadvantage of side looking radar systems. In the 1950s Synthetic aperture radar systems were invented (SAR). For images captured with SAR the azimuthal resolution was equal to half of the antenna length independent of range. A SAR system with a 3 m antenna at a 5 km range, the resolution would now become 1.5 m.

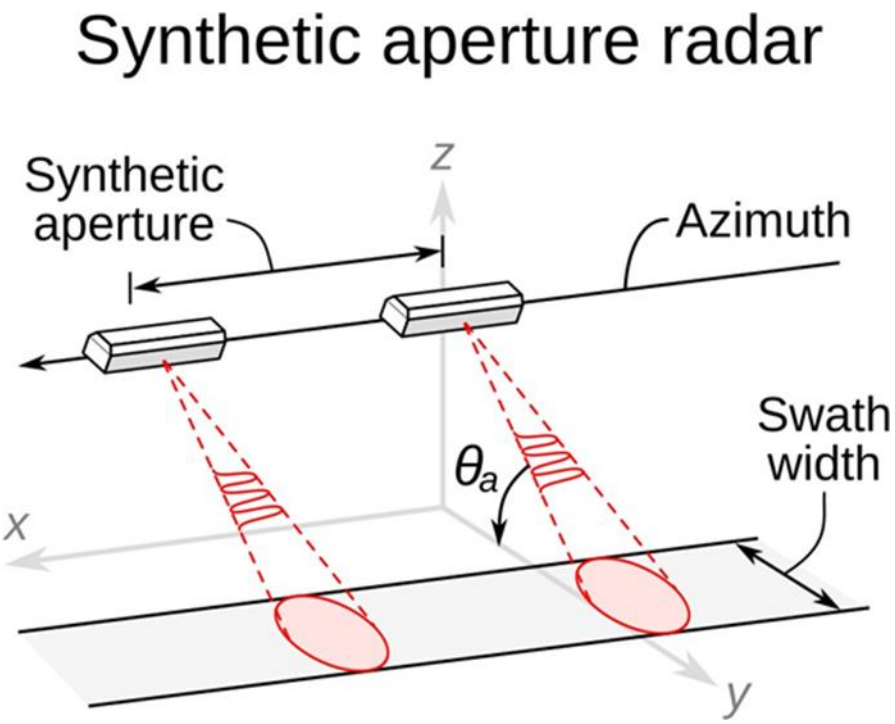

Figure 3. SAR Platform Moves in the X Direction and Records Backscatter from the Swath (Åmerbilly, 2021)

The azimuth (x) is the flight path of the platform, and the ground range (y) is the direction that is perpendicular to the flight path (Figure 3). The swath width is the extent of the image in the ground range direction and the length is determined by distance traveled with the radar turned

on. Consider Figure 4. At A, the SAR imaging system is positioned so that the object of interest is just outside the view of the radar. At B and C, the object is fully within the view of the radar. The system captures scatter from the object during B and C interval. At D, the different captures are added together. These positions are mathematically treated as if they were elements of a larger antenna (Ager, 2013; Campbell & Wynne, 2011; Lillesand, Kiefer, & Chipman, 2014). As the distance between the system and the object increases more elements along the flight path can receive backscatter because of the conical shape of the imaging area. This means that the azimuth resolutions are constant and independent of range (Lillesand, Kiefer, & Chipman, 2014).

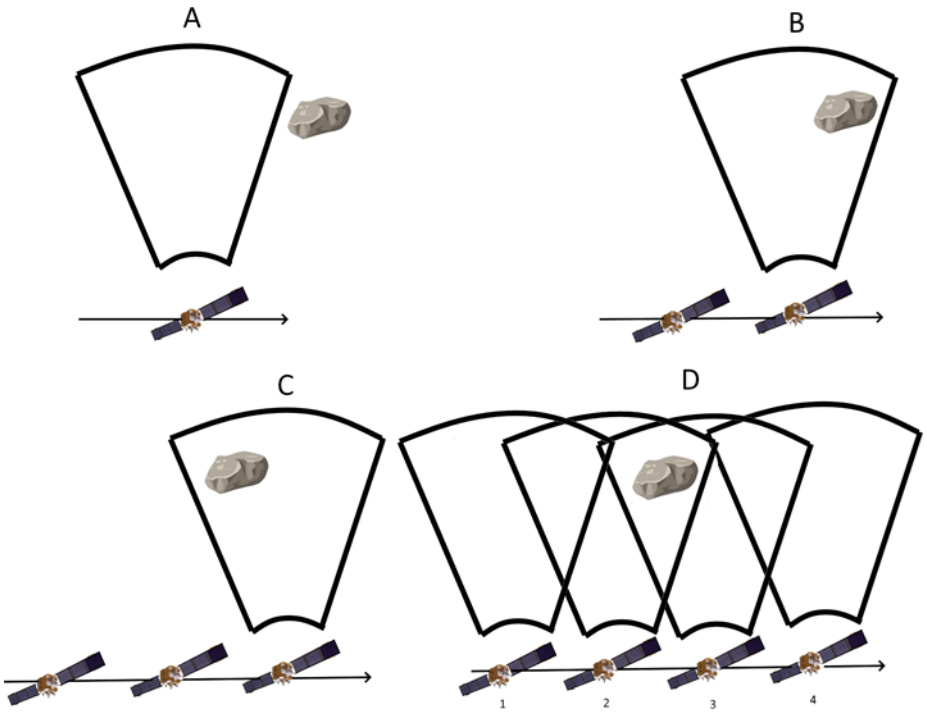

Figure 4. Different SAR Phases. In the Last Frame D, all the Recorded Scatter from the Different Phases is Complied (Åmerbilly, 2021)

The received signal is stored as single-look complexes (SLC), a SAR image where every pixel is corresponding to a resolution cell on the ground. These cells are sampled in azimuth and slant-range coordinate system. In the SLC format every cell has the complex *P* (Samiei-Esfahany, 2017)

$$P = \mathrm{Re}(P) + j\mathrm{Im}(P) = A \cdot \exp(j\psi)$$

where A is the pixel amplitude which is the square root of the signal return intensity, j is the imaginary unit. ψ is the phase of the received signal. A and ψ are related to the real and imaginary part of P as

$$\mathrm{Re}(P) = A\cos(\psi)\,, \qquad \mathrm{Im}(P) = A \cdot \sin(\psi)$$

The phase ψ is consists of the four components

$$\psi = W\{\psi^{range} + \psi^{atmo} + \psi^{scat} + \psi^{noise}\}$$

W: modulo-2π wrapping operator

ψ^{range}: Phase related to distance between cell on ground and position of radar sensor

ψ^{atmo}: Phase delay because of atmospheric effects

ψ^{scat}: Phase related to the distribution of scatterers within cell

ψ^{noise}: Phase due to system and thermal noise

There are different SAR acquisition modes and techniques such as Interferometric SAR (InSAR), Differential Interferometric SAR (DInSAR), and Polarimetric SAR (PolSAR), and their concepts and explanations can be found in textbooks and published papers (e.g., Moreira et al., 2013). These methods are used frequently to estimate millimetre-level deformations, generate deformation maps along railways, present time-series of the estimated deformations per measurement point, or integrate with other data for example, Airborne Light Detection and Ranging (LiDAR) and in-situ data. A non-comprehensive review of published studies about change detection of railways using the InSAR technique can be seen in Table 4. One of the important parameters in SAR systems is frequency bands, i.e., which part of the electromagnetic spectrum is used. Commonly used frequency bands in SAR systems are P, L, S, C, X, and K-band. Generally, penetration is the key factor for selecting the frequency bands. In other words, shorter frequency provides the stronger the penetration into vegetation and soil.

Table 4. Non-comprehensive review of published studies about change detection of railways using InSAR technique.

Authors	**Study area**	**Data**	**Temporal coverage**	**Method**	**Validation method**
Chen et al. (2021)	Along Beijing high-speed railway	**Envisat ASAR** (Descending) Band: C-band (5.6 cm) **TerrSAR-X** (Ascending) Band: X-band (3.1 cm)	18/06/2003–25/8/2010 27/05/2010–08/11/2015	Small Baseline Subset (SBAS) InSAR-derived subsidence method A new time series fusion method based on the minimum gradient difference of a fitting curve to produce time series subsidence.	Relationship between subsidence and hydrogeological factors
D'Amico et al. (2020)	Truss railway bridge overpassing the A14 Italian motorway	Sentinel 1A Band: 5.4 GHz COSMO-SkyMed Band: 9.6 GHz	04/2017–01/2018 03/2016–01/2018	Integration of the Ground Penetrating Radar (GPR) and InSAR	-----
Luo et al. (2011)	Beijing-Tianjin railway China	TerraSAR Band: X-band	2009/4/29 - 2010/11/11	InSAR-derived subsidence method by SARPROZ	-----
Ding et al. (2021)	Along the Lunan high-speed railway (East China)	Radarsat-2 Single Looking Complex (SLC)	2016 to 2018	Small Baseline Subset (SBAS)-InSAR	High-precision levelling results, groundwater level monitoring data

Singhroy et al. (2015)	Active high-risk surface deformation sites (like railway sites) in Canada	RADARSAT Constellation Mission (RCM)	2009-2011	InSAR	-----
Meng et al. (2021)	Zhangjiazhuang high-speed railway tunnel	Sentinel-1A IW	20 December 2015 and 6 February 2016 in an ascending orbit of 128	D-InSAR	Geological and geomorphological surveys, unmanned aerial vehicle image interpretation
Chang et al. (2016)	Railway network of the Netherlands, more than 3000 km long	Radarsat-2	2010-2015	InSAR	-----
Q. Zhang et al. (2019)	Qinghai–Tibet Railway	Advanced Synthetic Aperture Radar (**ASAR**) Band: C-band TerraSAR-X Band: X-band	2003-2012	Full rank matrix small baseline subset InSAR (FRAM-SBAS) timeseries analysis	GPS data
Poreh et al. (2016)	Campania, Italy (Railways, targeted bridge)	Cosmo-SkyMed (CSK) Band: X-band	2011/02/24-2015/03/23	DInSAR	The results were compared with temperature data.

Luo et al. (2017)	Jingjin Inter-City Railway, located in Tianjin, China.	TerraSAR-X Band: X-band	2009/04/29 - 2010/11/11	Multi-temporal InSAR (MT-InSAR) analysis	42 levelling points along the railway.
Hu et al. (2019a)	Zaltbommel, The Netherlands (10 km of railway)	RadarSAT-2 XF Airborne **LiDAR** product, Actueel Hoogtebestand Nederland 3 (AHN3)	March 2015 and August 2018	Multi-temporal InSAR (MT-InSAR) analysis and combining with LiDAR point clouds	----
Chang et al. (2020)	Betuwe freight train track, in the Netherlands (172 km)	Sentinel-1a/b (ascending) VV polarimetric channel Airborne **LiDAR** product, Actueel Hoogtebestand Nederland 3 (AHN3)	January 2017 and December 2019	Multi-temporal InSAR (MT-InSAR) analysis and combining with LiDAR point clouds	the in-situ track survey Rail Infrastructure Alignment Acquisition (RILA) measurements
Qin et al. (2017)	Railways of Beijing–Tianjin, Beijing–Shanghai, and Shanghai–Hangzhou	ENVISAT ASAR (ASAR) TerraSAR-X	2008/02/08-2009/12/04 2008/04/21-2012/10/05	Developing an improved PSI analysis approach	Comparing to the previous InSAR studies.

Bergevald (2019)	South of Gothenburg, Sweden	Sentinel-1 A and B Band: C-band TerraSAR-X	For DInSAR: 9 July 2018 (master) and 27 July 2018 (slave) 2 January 2016 and 7 September 2018	DInSAR Sentinel Application Toolbox (SNAP) software PSI analysis by SkyGeo from the TerraSAR-X	Comparing PSI and Optram

4.3. Interferometric Synthetic Aperture Radar (InSAR)

InSAR is a technique used to observe surface topography such as, subsidence, ground deformation, and glacier movements (Moreira et al., 2013). By observing the phase difference between two SAR images, the information about the position of a target, or the displacement during the time between acquisitions can be acquired (Samiei-Esfahany, 2017). The main ways that exist for gathering interferometric radar images are across-track or along-track. With across-track interferometry a moving platform equipped with bi-static antennas gathers radar data at the same time (Moreira et al., 2013). By using two antennas it is possible to obtain distance and angular measurements. The principal is similar to how humans use two eyes for depth perception (Hanssen, 2002). Another method is along-track interferometry or DInSAR, where a radar platform passes over the study area two or more times. The image pairs can now reveal changes that have taken place between passes. In this case a temporal baseline is established. Short temporal baselines can collect more rapid movements, such as movement of ships, while long temporal baselines can measure movement of glaciers (Campbell & Wynne, 2011). DInSAR can be operated from a bi-static platform with two antennas linearly along an orbital path or a mono-static platform in which a single antenna makes two or more orbits over the survey area (Campbell & Wynne, 2011; Yang, 2015).

An InSAR image is created by interfering two SAR images taken from different positions or different times, where the phase difference between these two SAR images is of interest. As mentioned earlier ψ^{range} is related to the distance between the cell on the ground and the radar; therefore, the phase difference between two SAR images can be exploited to calculate displacement between two acquisition times. The result of interfering two SAR images is another complex image called an interferogram. Due to the two SAR images being acquired from two slightly different positions, it is required to align the geometry of one image to the other. Then a complex conjugate multiplication is performed on the aligned SAR images (Samiei-Esfahany, 2017).

$$I = P_M {P^*}_S = A^M A^S exp\big(j(W\{\psi M - \psi S\})\big)$$

I: Constructed interferogram

P_M: SAR master

P_S: SAR slave

*: Complex conjugate

For a single pixel the interferometric phase can be written as

$$\phi_{MS} = W\{\phi^{range} + \phi^{atmo} + \phi^{scat} + \phi^{noise}\}$$

It is standard to explain phase by the degree of correlation between two SAR images, called coherence $|\gamma|\epsilon[0,1]$, where 0 means complete decorrelation and 1 means that robust deformation information can be generated. To generate accurate ground deformation, it is generally required to have a coherence index above 0.5 (Yang, 2015).

The dependent phase ϕ^{range} difference between the two SAR images is related to distance between the radar and the ground cell during the two acquisition times. This dependent phase can be divided into three different categories.

$$\phi^{range} = \phi^{flat} + \phi^{topo} + \phi^{defo}$$

The flat phase is caused by the curved reference surface of the earth and depends on viewing angle. The topographic phase is the effect of the surface height above the reference surface. This also is dependent on the viewing angle. The deformation phase is caused by the surface deformation between the two acquisitions. The flat and topographic phases can be removed by using orbit parameters and an external digital elevation model (DEM). This leaves the phase caused by the surface displacement.

$$\phi^{atmo} = \phi_M^{atmo} - \phi_S^{atmo}$$

Changes in atmospheric conditions between two SAR acquisitions will result in different atmospheric phases. These atmospheric delays are caused by turbulent processes in the atmosphere and different vertical refractivity properties.

$$\phi^{scat} = \phi_M^{scatt} - \phi_S^{scatt}$$

The scattering phase is induced by the difference in scattering behaviour between two SAR acquisitions. The scattering phase in each SAR image, is a function of the position of scatterers in a cell with respect to the radar and the electrical properties of the scatters. Decorrelation induced by scattering phase variation is divided into four categories. Baseline decorrelation is the result of different incidence angles between two SAR acquisitions. A ground cell on the ground seen by two radars at different angles will give different phase information. Doppler centroid decorrelation is similar to baseline decorrelation in that they are both caused by difference in incidence angles. Volumetric decorrelation is caused by scattering in 3D volumes such as tree canopies. Temporal decorrelation is the result scatterer variation due to changes on the ground, such as vegetation growth or rainfall. The noise phase is the result of noise induced by the radar system and post-processing operations.

If the atmospheric, scattering and noise phase difference were zero, then a coherent image would be made, and the interferometric phase would only depend on the change of travel time of the signal between sensor and pixel phase. But this is often not the case. The main challenge when using InSAR is the ability to extract coherent data from noisy interferometric phases. To manage the limitations of InSAR, a technique called Multi-Temporal InSAR (MT-InSAR) was developed to manage decorrelation.

4.4. Multi-Temporal InSAR (MT-InSAR)

MT-InSAR techniques focus on tackling decorrelation to produce deformation results (Minh, Hanssen, & Rocca, 2020). Two main approaches were developed. One to observe isolated pixels which do not suffer from decorrelation and then using these to extract deformation information. The other approach uses pixels affected by decorrelation and applies different filters and processes to reduce decorrelation. The first one is called the persistent scatterers interferometry (PSI), which was first introduced by Ferretti et al. (2001), and the second is

distributed scatterers interferometry (DSI) (Samiei-Esfahany, 2017). There is also a combination of both. Due to the availability of historic SAR data, it is possible to study temporal displacement over a large time span by utilising large stacks of SAR images.

MT-InSAR, can be useful for monitoring structural health along railway systems over time (Hu et al., 2019a). This technique is suitable for railways due to its high precision accuracy and uses multi-temporal SAR data (Hu et al. 2019a). MT-InSAR can be used to reduce the atmospheric delays and decorrelation noise in DInSAR (Hu et al., 2019b). Wasowski & Bovenga (2014) provides a review of various MT-InSAR applications and a method for using MT-InSAR to investigate landslides and unstable slopes. MT-InSAR is opportunistic as it provides valuable information where other data may not be available. This paper was published before the launch of Sentinel-1, but the authors foresee that Sentinel-1 will guarantee more efficient uses of MT-InSAR for landslide investigations. X-band data provides high spatial resolution imagery at a reduced revisit time and short wavelengths. This allows for higher temporal resolution for hazard monitoring, improvements in detecting structural stability of railways, and the possibility to generate more accurate DEMs.

Persistent Scatterers

For SAR images the value for each pixel is the sum of the returns from the scatterers on the ground. If these move in relation to each other between satellite passes, then the phase return will vary randomly which causes decorrelation. If a pixel is instead dominated by one stable scatterer that has a high signal to noise-ratio, the variance becomes small enough to enable the extraction of deformation phase (Hooper, 2007). It only takes into consideration the phase information from stable backscatters in order to maintain coherence. This means that $\Phi^{s}cat$ is small over a large temporal and perpendicular baseline. This enables the extraction of information from a stack of interferograms. For PSI one image is chosen as master and all other images are referenced to it. Stable backscatterers, referred to as persistent scatterers, can be buildings, bridges or large rocks which are strong reflecting objects and are constant (Crosetto et al., 2015; Yhokha et al., 2018).

Distributed Scatterers

The idea behind distributed scatterers is to use interferogram pairs with minimal spatial and temporal baselines between acquisitions (Pawluszek-Filipaik & Borowski, 2020). DSI does not use single master stack. Instead, they are arranged in subset network configurations. This reduces the decorrelation that occur with long baselines. Distributed scatterers technique is usually used when the surface is comprised of soil, vegetation, and non-built-up areas (Minh, Hanssen, & Rocca, 2020).

4.5. Satellite's Relevant for InSAR Processing

There are various satellites launched by space agencies around the world that contain a SAR sensor; each with different temporal, spatial, and spectral resolutions. One of the most recent launches was by the European Space Agency (ESA) which launched a constellation known as Sentinel-1 as part of the Copernicus Program. The Copernicus Program was launched in 2014 and branded as "*Europe's Eyes on Earth*" (European Commission, 2015, p.4). The purpose is to provide open-source data that is both timely and easy to use/access (European Commission, 2015). Copernicus consists of six thematic streams: atmospheric monitoring,

marine environment monitoring, land monitoring, climate change, emergency management, and security (European Commission, 2015). Sentinel-1 consists of two satellites: Sentinel-1A and Sentinel-1B that were launched in 2014 and 2016 respectively (European Space Agency, n.d.). The satellites operate under the C-band, a frequency within the microwave portion of the electromagnetic spectrum. This is significant because microwaves can penetrate clouds meaning imagery is provided in any weather condition, all day and night (European Space Agency, n.d.). Each satellite has a temporal scale of 12 days, resulting in available imagery around every 6th day or less.

Other common satellites that are often utilised for research are TerraSAR-X a German satellite that operates under the X-band of the microwave spectrum and Radarsat-2, a satellite launched by the Canadian Space Agency that uses the C-band. Along with the C-band and X-band another band in the microwave spectrum is the L-band. The X-band is the shortest wavelength followed by the C-band, and then L-band (Wempen & McCarter, 2017). P, S, and K-bands are also sometimes used. Longer wavelengths have the capability to penetrate dry soil, ice, or vegetation but shorter wavelengths are better at detecting smaller changes in the surface over time (Wempen & McCarter, 2017). Some studies use acquisitions from multiple satellites, for instance TerraSAR-X and Sentinel-1A in order to combine different bands to enhance the ability of deformation modeling (Z. Zhang et al., 2019). Figure 5 below gives an overview other historical and current satellite sensors used.

SENSOR	OPERATION	FREQUENCY BAND (POLARIZATION)	COMMENTS	INSTITUTION, COUNTRY
Seasat	1978	L (HH)	First civilian SAR satellite, operation for only ca. three months	NASA/JPL, USA
ERS-1/2	1991–2000/ 1995–2011	C (VV)	European Remote Sensing Satellites (first European SAR satellites)	ESA, Europe
J-ERS-1	1992–1998	L (HH)	Japanese Earth Resource Satellite (first Japanese SAR satellite)	JAXA, Japan
SIR-C/ X-SAR	April and October 1994	L & C (quad) X (VV)	Shuttle imaging radar mission, first demonstration of spaceborne multi-frequency SAR	NASA/JPL, USA DLR, Germany ASI, Italy
Radarsat-1	1995–today	C (HH)	First Canadian SAR satellite, swath width of up to 500 km with ScanSAR imaging mode	CSA, Canada
SRTM	Feb. 2000	C (HH+VV) and X (VV)	Shuttle Radar Topography Mission, first spaceborne interferometric SAR	NASA/JPL, USA DLR, Germany ASI, Italy
ENVISAT/ ASAR	2002–2012	C (dual)	First SAR satellite with Transmit/Receive module technology, swath width up to 400 km	ESA, Europe
ALOS/PalSAR	2006–2011	L (quad)	Advanced Land Observing Satellite (Daichi), swath width up to 360 km	JAXA, Japan
TerraSAR-X/ TanDEM-X	2007–today 2010–today	X (quad)	First bi-static radar in space, resolution up to 1 m, global topography available by end of 2014	DLR/Astrium, Germany
Radarsat-2	2007–today	C (quad)	Resolution up to: 1 m × 3 m (azimuth × range), swath width up to 500 km	CSA, Canada
COSMO-SkyMed-1/4	2007 … 2010–today	X (dual)	Constellation of four satellites, up to 1 m resolution	ASI/MiD, Italy
RISAT-1	2012–today	C (quad)	Follow-on satellite (RISAT-1a) to be launched in 2016, RISAT-3 (L-band) in development	ISRO, India
HJ-1C	2012–today	S (VV)	Constellation of four satellites, first satellite launched in 2012	CRESDA/CAST/ NRSCC, China
Kompsat-5	Launch scheduled in 2013	X (dual)	Korea Multi-Purpose Satellite 5, resolution up to 1 m	KARI, Korea
PAZ	Launch scheduled in 2013	X (quad)	Constellation with TerraSAR-X and TanDEM-X planned	CDTI, Spain
ALOS-2	Launch scheduled in 2013	L (quad)	Resolution up to: 1 m × 3 m (azimuth × range), swath width up to 490 km	JAXA, Japan
Sentinel-1a/1b	Launch scheduled in 2013/2015	C (dual)	Constellation of two satellites, swath width up to 400 km	ESA, Europe
Radarsat Constella-tion-1/2/3	Launch scheduled in 2017	C (quad)	Constellation of three satellites, swath width up to 500 km	CSA, Canada
SAOCOM-1/2	Launch scheduled in 2014/2015	L (quad)	Constellation of two satellites, fully polarimetric	CONAE, Argentina

Figure 5.Overview of Other Satellite Sensors used Globally (Moreira et al., 2013)

5. Interferometric Synthetic Aperture Radar (InSAR) Applications

An extensive literature review was done in order to assess InSAR technology. The previous chapter highlighted the theoretical background surrounding InSAR, the various techniques, and satellite sensors that can be used for InSAR analyses. This chapter delves into some of the many different applications for using InSAR.

Based on the increasing concern of climate change and how it will affect the transportation sector, and the corresponding track geometry changes, InSAR, can be useful for monitoring various aspects affected by climate, such as permafrost melt, temperature, and landslides. The results from InSAR monitoring techniques can be used to interpret changes in the climate and predict how railway infrastructure and operations will be impacted in the future. Track geometry can also be affected by urban development, therefore InSAR in general can be a useful tool in risk management as it can be used to identify at risk areas among other uses.

5.1. Permafrost Monitoring using InSAR

A study by Zhao et al. (2016) describes permafrost and its relationship to the environment. Permafrost has serious implications on regional and global water circulation, climate warming, carbon deposit, and influences ecology, biogeochemical, and geophysical processes in cold regions around the world. It is important to monitor surface deformation over permafrost regions as understanding the dynamic processes and assessing the role of climate change will help to prevent potential damage to engineering structures, such as railways, that are situated over permafrost. Permafrost is unique in that it interacts with the atmosphere, pedosphere, and lithosphere, is subject to seasonal deformation, and is influenced by seasonal environmental factors such as air temperature, precipitation, ground temperature, and solar radiation. The frozen soils in permafrost regions typically experience natural seasonal uplift (frost heave) and subsidence (thaw settlement). Active layer thickness is the main determining factor of permafrost moving and is usually monitored using probing, in-situ temperature sensors, or satellite imagery (Schaefer et al., 2015). Air temperatures above the Arctic Circle are rapidly increasing at approximately twice the global average resulting in permafrost melt and deeper active layers (Schaefer et al., 2015). This in turn can lead to ground instability and subsidence of structures such as buildings or railways.

The Qinghai-Tibet Railway (QTR) is located on the Qinghai-Tibet Plateau in China and is known for being the highest altitude railway in the world and is underlain with permafrost (Q. Zhang et al., 2019). Many studies have been conducted on this line to monitor ground subsidence. Zhao et al. (2019) uses the SBAS technique to monitor ground deformation with an emphasis on climatic factors modeling (specifically, air temperature and precipitation). Results concluded that surface deformation over frozen soil is negatively correlated to precipitation and air temperature. Additionally, they examined a time lag of 60 days between maximum ground subsidence and the highest air temperature. Q. Zhang et al. (2019) used a Full Rank Matrix SBAS (FRAM-SBAS) time-series analysis using TerraSAR-X images to analyse the QTR before construction of the rail, and after the opening. The main conclusion of the study indicates that deformation was small before opening the railway and although it is still considered relatively stable today, it is important to continue monitoring the area due to geological hazards in the region that could quickly change deformation rates.

Z. Zhang et al. (2019) used a combination of TerraSAR-X and Sentinel-1A satellites and extended time-series InSAR methods to monitor the deformation of the QTR; combining X- and C- band data to enhance the ability of deformation modeling. The study mentioned that

permafrost and mountainous regions can be associated with harsher environments which in turn can lead to difficulties monitoring subsidence in the field. Furthermore, the authors discussed that when working with permafrost it is important to note the challenges with temporal variation as permafrost and therefore land subsidence changes greatly between summer and winter.

Johansson et al. (2011) conducted a study regarding permafrost in Abisko National Park, an area Malmbanan runs through. Here there are areas that are underlain with discontinuous/sporadic permafrost, and active layer thickness has been monitored since 1978 This study focused on redrilling old boreholes to determine the mean annual ground temperatures and active layer thickness. It was concluded that the increasing mean annual ground temperatures in the area has been leading to an increase in active layer thickness, making Abisko vulnerable to climate change in the future. This prediction may lead to increasing instability of the railway and ground surrounding the railway, solidifying the importance of monitoring ground subsidence along Malmbanan.

5.2. Landslide and Flood Monitoring using InSAR

InSAR can also be used for monitoring landslides and identifying areas of high risk to prepare for the future (Deng, 2010). It can be used to provide insight into a landslides state of activity and velocity (Journault et al., 2018). Additionally, it can give information on landslide deformation at local and regional scales (Journault et al., 2018). In Scandinavia it is predicted that there will be an increase in precipitation and temperature in the coming years leading to high vulnerability of urban areas, particularly road infrastructure (Ahlmer et al., 2018). Therefore, monitoring soil moisture using SAR imagery can be a useful tool in predicting and monitoring landslides.

Active acquisitions can also be matched with passive satellite images. For instance, the Landsat satellite launched by NASA can be used to monitor land use changes, before and after a major flooding or landslide event (Bonn & Dixon, 2005). Colesanti and Wasowski (2006) joins C- and L-band small baseline SAR interferometry to investigate the current and potential uses of InSAR for landslide assessment. This study is focused on the Alps in Lichtenstein. The study concluded there are several requirements for the application of using InSAR for landslide monitoring which include: bare surfaces, slow movements, “coherent” landslides with little internal deformation, low to moderate slope inclination, and slope orientation should be suitable in respect to the SAR viewing angle. Journault et al. (2018) conducted a study in Ashcroft, B.C., Canada measuring landslide displacements along the Thompson River Valley. The study uses PSI techniques to monitor the displacement of multiple landslides in the area and to classify their movement as either an active state of activity, dormant state, or extremely slow velocities. The study concluded that in the Thompson River Valley landslides display seasonal changes in their rate of displacement. It was found that landslides showed more displacements during the late fall and winter months compared to spring and summer.

Additionally, due to climate change, some regions are subject to more intense rainfall, therefore InSAR can be used to map the flooding extents (Zhou et al., 2018; Zhang et al., 2018). Due to SAR’s capabilities to operate under any weather conditions, it is possible to acquire imagery before, during, and after a major rainfall event, allowing for full flood extent mapping which can be used to identify and monitor risk areas (Zhang et al., 2018).

5.3. Temperature Monitoring using InSAR and Other Passive Satellites

One of the consequences of the increased temperatures associated with climate change for railway infrastructure is track buckling. Dobney et al. (2009) presents a study which attempts to quantify the effects of high temperatures in the summer due to climate change on buckling and rail delays in south-east United Kingdom. Climate change is predicted to increase summer temperatures in the U.K., particularly in the south-east region, leading to an annual increase in rail buckles and therefore traffic delays. A buckle is defined as a deviation in track alignment that is serious enough to potentially cause derailment. Therefore, there is a potential for using satellite imagery to detecting changes in railway infrastructure due to heat.

To gain information specifically about temperature, changes in land surface temperature (LST) can be monitored using either passive or active satellite data. LST is the temperature measured at the surface level and is often regarded as the skin temperature of the ground (Dash et al. 2001). Regarding remote sensing, it is defined as the average temperatures of the different surface types in each pixel and is weighted by their fractional cover (Dash et al. 2001). Landsat 7 and 8 has specific thermal infrared bands which have the capability to report the temperature of the ground which is typically hotter than the atmosphere (NASA, 2020).

Avdan and Jovanovska (2016) developed an algorithm for mapping LST using Landsat 8 data that could potentially be useful for monitoring the surface temperature of the railway tracks over time in relation to track buckling and climate change. They used a combination of NDVI, emissivity, and radiance to create a model used for calculating LST with positive results (Avdan & Jovanovska, 2016). A study conducted by Walawender et al. (2013) used Landsat imagery to investigate the thermal contrast between the city of Krakow, Poland, and the surrounding area. Through this study it was determined that this contrast was most visible in July when the air temperature was also the highest, due to the greater heat storage and specific thermal properties (heat capacity and conductivity) of urban surfaces of man-made materials. It was concluded that LST was highest in urban fabric, industrial, and commercial zones, including the airport and railways. Crosetto et al. (2015) discusses the ability to measure thermal expansion using X-band PSI observations. A big advantage of PSI is that it is sensitive to small deformations, including those caused by thermal expansion, therefore showing high accuracy results. This paper focuses on thermal expansion of buildings but could have the potential to be expanded to other areas. The main outcomes of this study concluded that X-band PSI is useful for making thermal maps to highlight different expansion behaviours. However, if the thermal expansion is not explicitly modelled, PSI deformations may be affected by distortions which particularly occur when limited PSI datasets in short time periods are analysed. There are still limitations surrounding the retrieval of LST from satellites. They include: the need for atmospheric correction, challenges with the albedo effect, and there are many ways to physically interpret LST (Li et al., 2014).

5.4. InSAR in Combination with Other Techniques

InSAR can be linked with other techniques such as light detection and ranging (LiDAR), ground penetrating radar (GDR), and leveling. LiDAR uses lasers to measure the elevation of objects (Hu et al., 2019a). Additionally, it can be used to overcome limitations of MT-InSAR by measuring the exact position of radar scatterers (Hu et al., 2019a). LiDAR can also be used to classify the scatterers which in turn makes it easier to interpret deformation signals (Hu et al. 2019a).

Tosti et al. (2020) provides a newer study on the combination of InSAR with a well-established non-destructive testing technology known as Ground Penetrating Radar (GPR). InSAR is

useful for detecting areas where subsidence is occurring, while GPR can be used to diagnose the causes of deformation. In short, GPR gives information about structures within a surface, usually the ground, to be implied by the transmission and reception of electromagnetic waves (EM). When a physical discontinuity is detected, the EM waves are partially back reflected to the receiver. This then allows for reconstruction of features of the subsurface. A fusion of the two technologies allows for more comprehensive assessment of the infrastructure being monitored.

Fryksten and Nilfouroushan (2019) used Sentinel-1 data and precise leveling data to analyse land subsidence in Uppsala, Sweden. PSI was used to map ongoing ground deformation and leveling was used to validate these results. The study concluded that Sentinel-1 together with PSI is useful and reliable. Luo, Zhou, and Perissin (2017) conclude similar results by monitoring subsidence of a high-speed railway in China using a TerraSAR-X MT-InSAR analysis. Serrano-Juan et al. (2017) compares levelling with InSAR to monitor the dewatering of underground construction sites. They conclude that InSAR is useful for investigating where there are deformation issues, whereas levelling is better suited for quantifying the impact on nearby buildings.

5.5. Swedish Ground Motion Service

Ground motion or deformation measurement and monitoring are key factors in risk assessment and management. This type of information has many applications. For example, it helps both the private and public sector have a better understanding of ground motion in order to effectively plan projects, protect their assets on local and regional scales, and in some cases even save lives. Repeated precise leveling and GNSS measurements on control points have been common geodetic techniques to measure and to map the ground deformation. In Sweden, InSAR has been used to monitor the local ground deformation in several places. For example, the ground deformation in and around the Kiruna mine in northern Sweden has been studied (Baduge et al., 2016). Moreover, the ground subsidence in two other cities i.e., Uppsala and Gävle has been investigated using InSAR and has been validated with local observations and precise levelling (Fryksten & Nilfouroushan, 2019; Gido et al., 2020).

At a larger scale, several countries in Europe have developed or are in process of developing nation-wide InSAR services to monitor the ground motion covering the whole country. For example, Denmark, Italy, Netherland, Germany, and Norway have produced the deformation map of the whole country using Sentinel-1 satellite radar images. In Sweden, a collaboration between several Swedish organisations (SNSA, Trafikverket, Lantmäteriet, SGI, SGU, Chalmers University and FOI) and Norwegian Geological survey (NGU) has started last year to introduce a nationwide ground motion service (GMS) for Sweden that is based on Sentinel-1 satellite data and has the potential to be used in several areas such as climate adaptation, spatial planning, and infrastructure monitoring. The online service not only shows the ground motion for billions of measurement points but also shows the temporal changes of the deformation at these points during the period of 2015-2021. During this project, validation and evaluation of public benefit will be carried out to provide a recommendation for whether a corresponding service should be introduced permanently or not. The main goals of the project are as following:

- To cover the entire country (excluding the forest and vegetated areas where InSAR has limitation) and have a large-scale picture of deformation with mm-cm accuracy
- To highlight risk zones (e.g., subsiding zones and landslides) in different parts of the country

- To monitor the structural stability of infrastructure (e.g., urban bridges, hospitals, and embankment dams)
- To secure and effectively plan future infrastructures (e.g., tunnels, railways, railways, roads, and chemical factories)
- To find local deformations which affect geodetic infrastructure (e.g., geodetic benchmarks, SWEPOS GNSS stations)

The initial plan is to make the online Swedish GMS service publicly available in autumn 2021 and for it to be updated by NGU next year.

6. Malmbanan as a Case Study

Malmbanan is a heavily used and studied railway line in Northern Sweden and Norway running between Luleå, Sweden and Narvik, Norway (Figure 6). It is used primarily for transporting iron-ore from mines in Sweden to the ports of Luleå and Narvik. For the purpose of this study, the area is narrowed down to the section between Kiruna and Riksgränsen, the border to Norway.

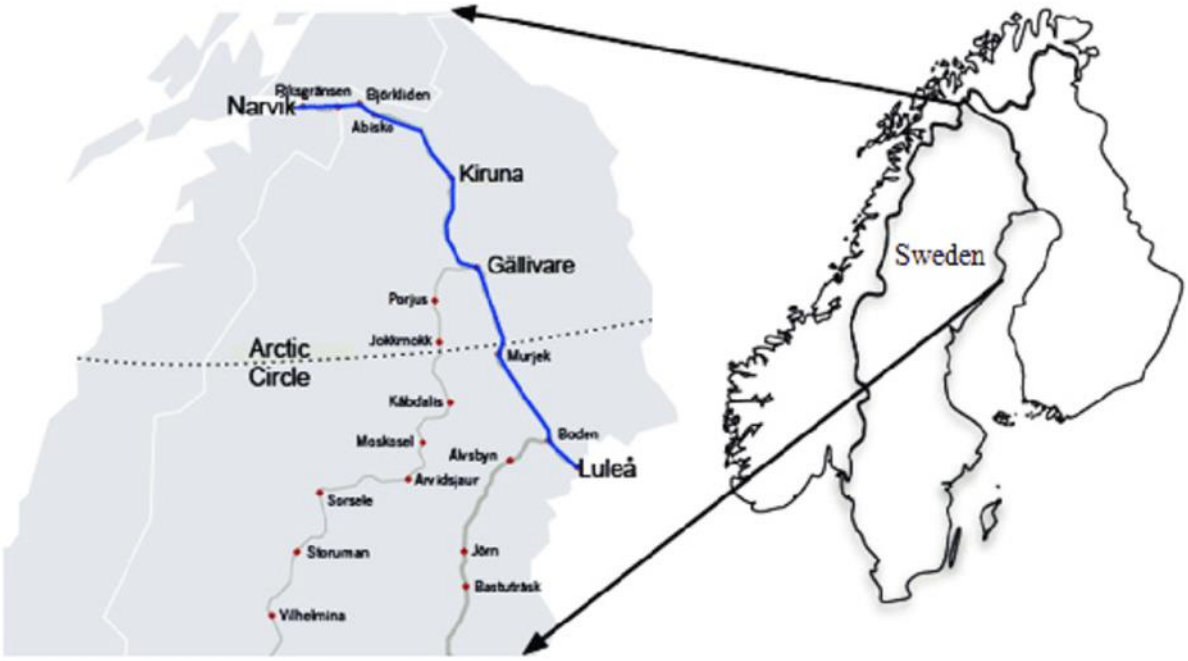

Figure 6. Map of the Geographical Location of Malmbanan (Lin, 2013)

Malmbanan is an electrified single-track railway line with a maximum load of 30 metric tons, the only line in Sweden with this load capacity. Demands on this route are increasing as longer and heavier trains are operating on the tracks, therefore increasing the performance requirements (Nordmark & Larsson-Kråik, 2007; Trafikverket, 2021b). Furthermore, this line has the largest predicted traffic increase of all railway lines across Sweden, with an expected growth rate of 136% between 2006-2050 (Asplund et al., 2014).

This line is located above the Arctic Circle where the mean temperature ranges between 14 °C and +14 °C (SMHI, 2020). The line runs through rough terrains such as high mountains, terraces on fjords, and peat (Larsson-Kråik, 2012), and can be divided into three parts depending on prevailing soil type. The first third (closer to Luleå) consists mostly of till and peat. The second is a transition into till and bare rock and the last third which is close to the Norwegian border is mostly rock (Figure 7). The soil depth ranges up to 38 m halfway along the railroad according to data from the Geological Survey of Sweden (Figure 8).

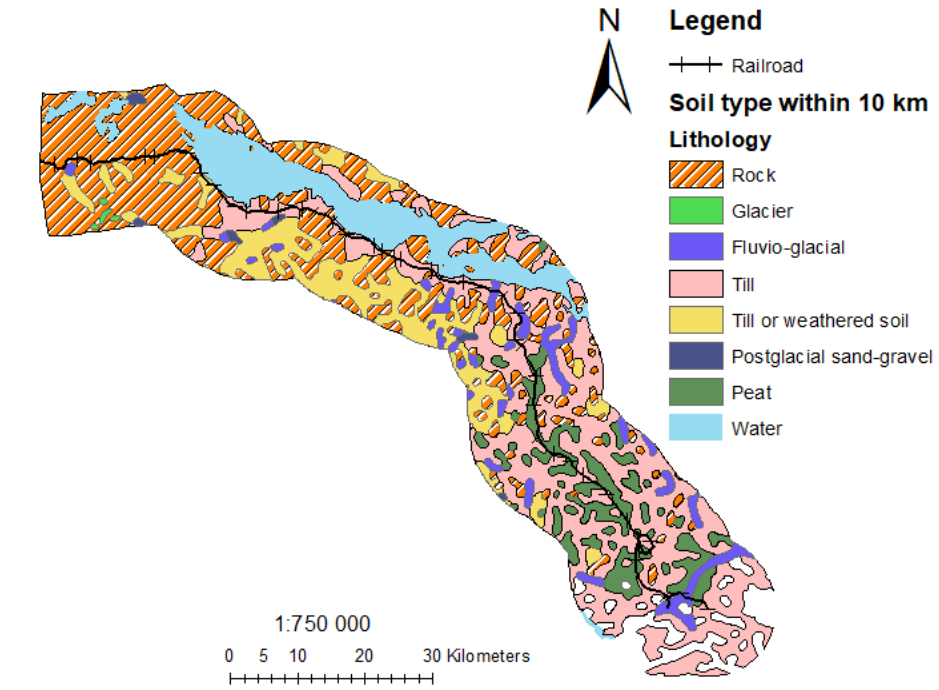

Figure 7. Soil Type within 10 km Distance to the Railroad Kiruna-Riksgränsen (SGU, 2021)

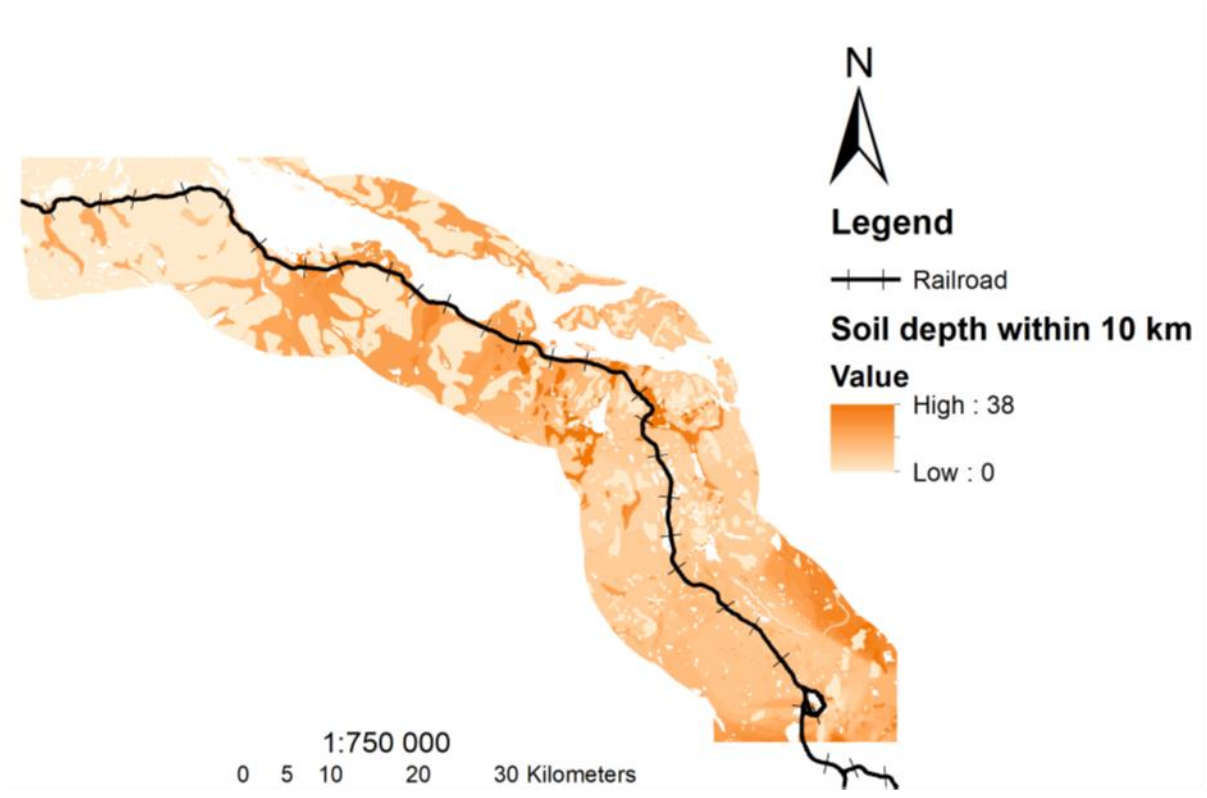

Figure 8. Soil Depth within 10km Distance to the Railroad Kiruna-Riksgränsen (SGU, 2021)

6.1. Vertical and Horizontal Velocities Detected with InSAR along Malmbanan

In order to detect the vertical and horizontal velocities along Malmbanan, Sentinel-1 A and B Satellite data (C-band) from the European Space Agency (ESA), which is freely available through the Copernicus Open Access, were used. Datasets containing Single Look Complex (SLC) imagery of both ascending and descending geometries for the time-period of 27 September 2015 – 26 June 2020, covering about 8,863 km^2, were processed in ENVI SARScape software using the Permanent Scatter Informetric (PSI) technique (Ferretti et al, 2001; Hooper et al., 2007) to quantify ground surface deformation over the study area. The raw data was collected and processed by Trafikverket and SWECO.

After the data processing in SARScape, time series of ground surface velocities, in both vertical and horizontal dimensions, for 529,142 points scattered at ~10 m distance over the study area were generated. The time step of the generated data series was 12 days from the beginning until September 21, 2016, and then reduced to 6 days for the rest of the period. As we were interested in ground surface movements under the railway, we extracted velocities (vertical and horizontal) at the InSAR PS points close to the railway. This was done in ArcMAP via joining the clipping respective layers, and the average distance of Optram points to closest InSAR PS points was about 5.7 m. Then hotspot points showing high velocities were identified.

The vertical velocity map shows both subsidence and uplift within an 800-metre-wide corridor with the railroad Kiruna-Riksgränsen as the centreline (Figure 9). The dominant range for the derived velocities was on average between -10 mm/year (subsidence) to +10 mm/year (uplift). Vertical displacements with greater rates were also observed at some specific areas such as the large subsidence close to Kirunavaara, Björkliden, and Riksgränsen (-25 mm/year) (Figure 10).

Horizontal velocity of the displacements was up to 10 mm/year over large areas in both east and west directions. The eastward displacements were mainly observed between Kiruna and Kaisepakte and the westward displacements between Kaisepakte and Riksgränsen (Figure 10).

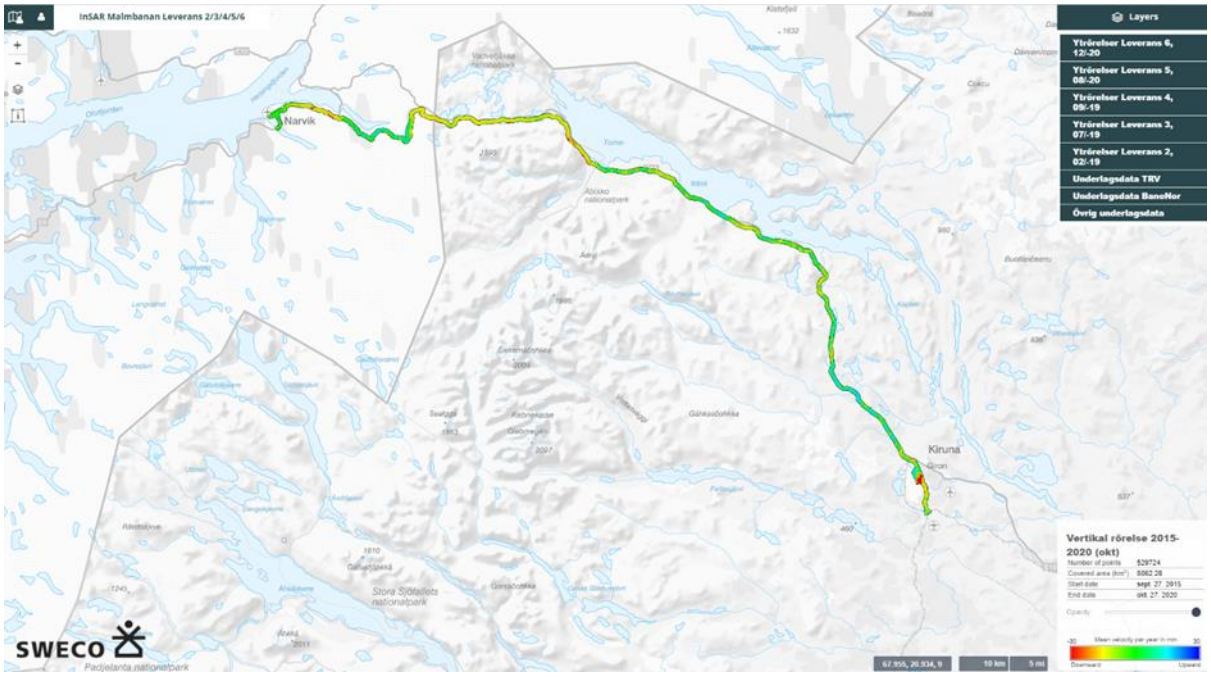

Figure 9. InSAR-derived Mean Vertical Velocity (mm/year), 2015-2020, Within 400 m Distance to the Railroad Kiruna-Riksgränsen, The Map was generated by SWECO in cooperation with EDInsights

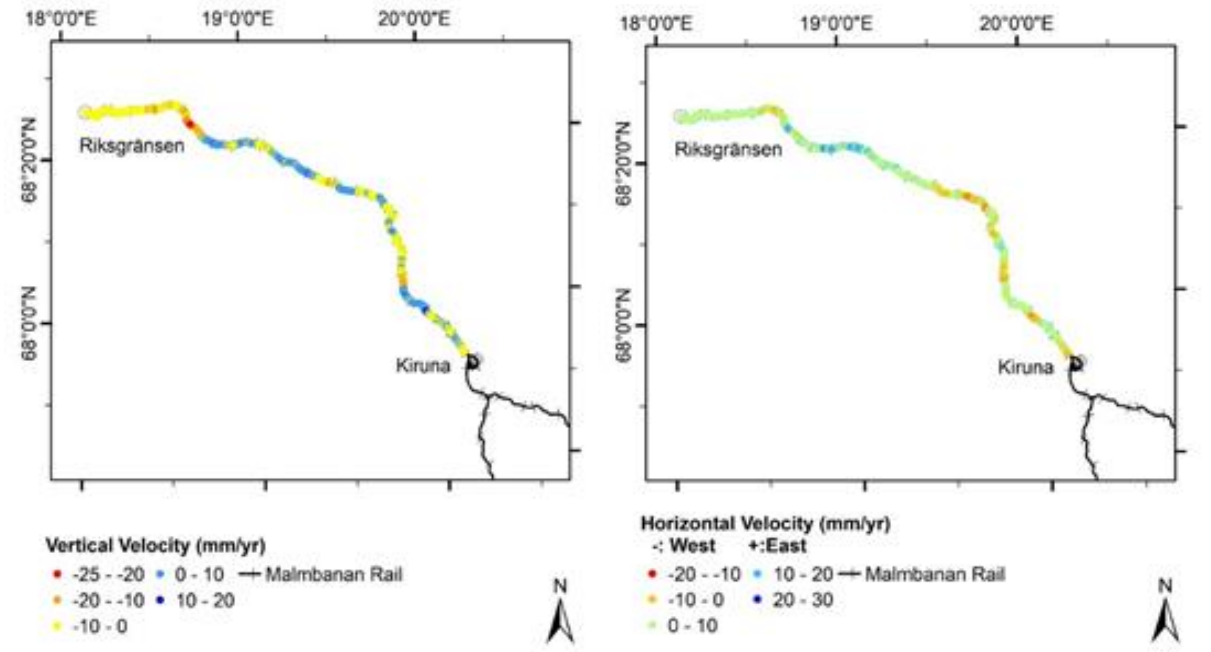

Figure 10. InSAR-derived Mean Vertical Velocity and Mean Horizontal Velocity (mm/year), 2015-2020, at the Optram Points Along the Railroad Kiruna-Riksgränsen. For the subfigure on the horizontal velocity (to the right): Negative = Westward Velocity and Positive = Eastward Velocity

Table 5 shows some of the hotspot locations (KM Tavla) with major displacements (vertical and horizontal) identified over the area between Kiruna and Riksgränsen. For one of the identified hotspots, the KM Tavla 1513/802 close to Björkliden, the vertical velocity map of the surrounding area and a time-series of the vertical displacement, 2015-2020, are respectively

shown in Figure 11 and Figure 12. Figure 13 indicates that there is physical evidence of track settlement along some parts of the railway track.

Table 5. Hotspot Locations with Major Displacement as Identified by InSAR, 2015-2020, in the Study Area (Kiruna-Riksgränsen, Sweden. (Source: SWECO)

Vertical direction (”-”=downward, ”+”=upward)					
	Mean velocity, 2015-2020 (mm/yr)		Mean velocity only for 2020 (mm/6 months)		Total displacement 2015-2020 (mm)
KM Tavla 1513/802	-23.4	KM Tavla 1451/358	-35.9	KM Tavla 1513/802	-118.6
KM Tavla 1513/855	-23.4	KM Tavla 1453/491	-33.9	KM Tavla 1513/855	-118.2
KM Tavla 1529/490	-19.1	KM Tavla 1553/542	-33.6	KM Tavla 1513/750	-98.3
Horizontal direction (”-”=westward, ”+”=eastward)					
KM Tavla 1502/194	+24.8	KM Tavla 1466/342	-32.7	KM Tavla 1502/194	+115.8
KM Tavla 1502/248	+23.9	KM Tavla 1484/250	+32.4	KM Tavla 1502/248	+110.6
KM Tavla 1502/300	+20.4	KM Tavla 1466/86	-29.6	KM Tavla 1496/328	+91.4

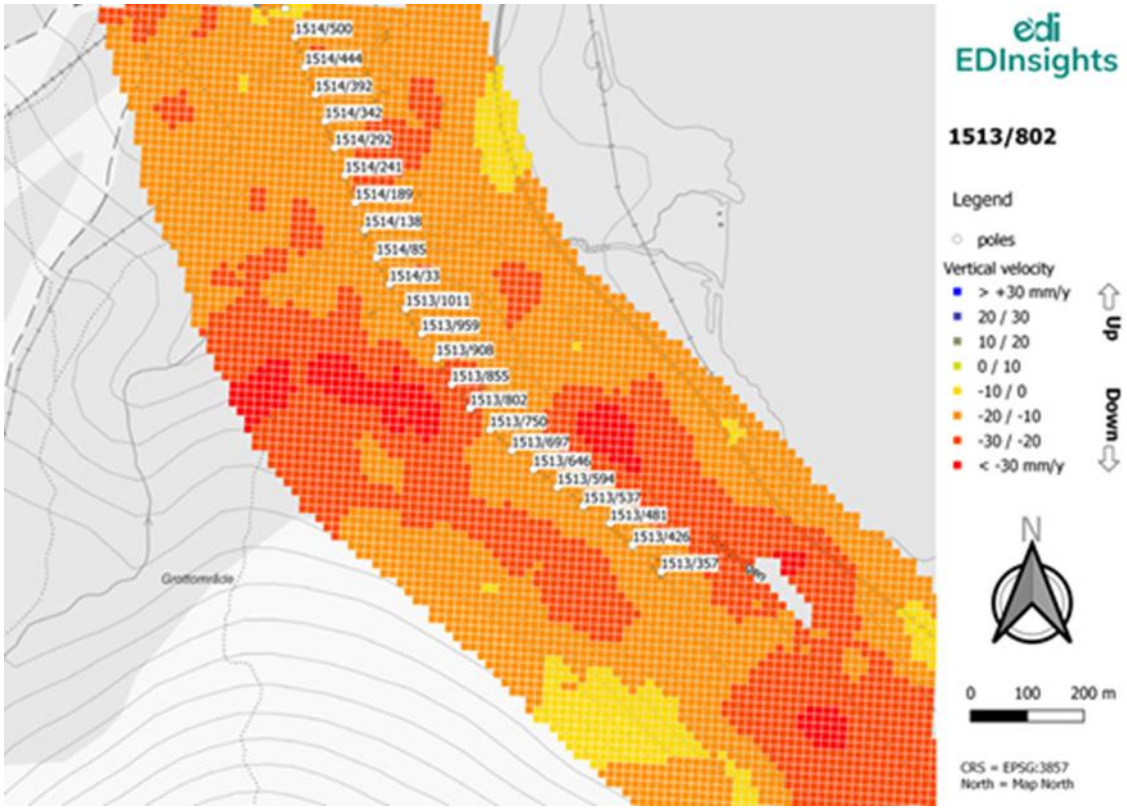

Figure 11. An Identified Hotspot Area (including KM Tavla 1513/802 Station) with Major Displacement in the Study Area. The map shows mean vertical velocity (mm/year) derived by InSAR, 2015-2020 (SWECO)

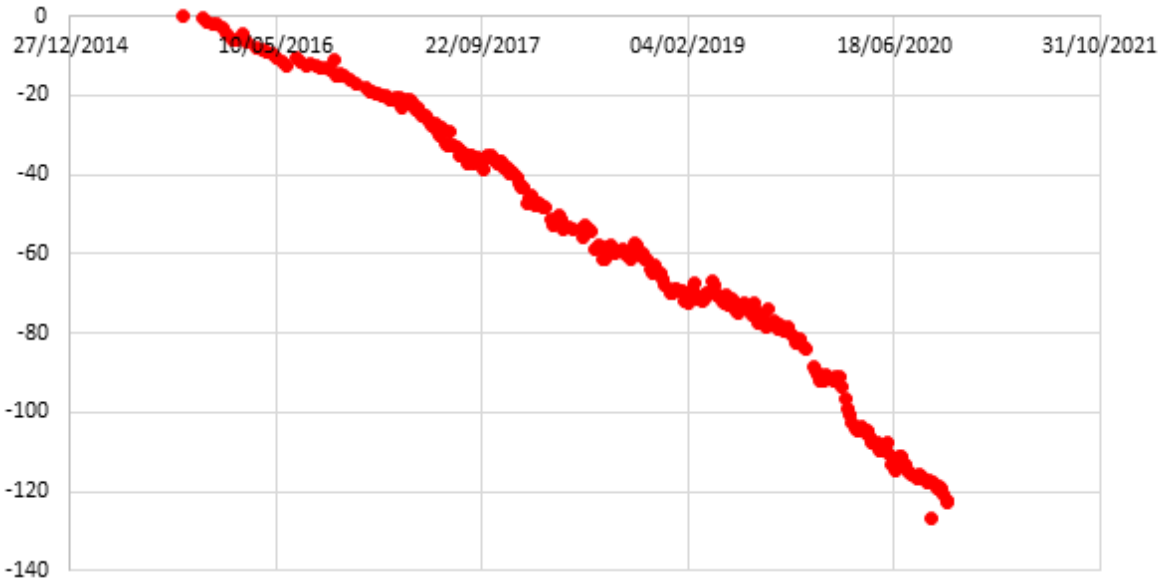

Figure 12. Time Series of Vertical Displacement (mm) Derived by InSAR, 2015-2020, at the Hotspot Station KM Tavla 1513/802 in the Study Area

Figure 13. Track Settlement along Malmbanan Track, reprinted with permission (photograph: Tony Armstrand, Trafikverket)

6.2. Classification of InSAR and Optram

In order to compare the InSAR-derived results with those from Optram, we developed a method including the following steps. First, we aggregated and matched the two datasets. Secondly, we identified areas with significant changes over time in both Optram and InSAR. Thirdly, we calculated the probability of overlapped changes for the two monitoring techniques. Lastly, a sensitivity analysis was done to study how the selection of different parameters and thresholds affected the result. In these steps, 31 different tests were conducted with various combinations of different time periods, section lengths, and thresholds in order to determine the changes in correlation between InSAR and Optram. A more in-depth description of the methods and the results from the 31 different tests can be found in Appendix A.

In the first step, the InSAR and Optram datasets both contained GPS locations for every measurement which allowed us to match these two sets. Because every Optram measurement comes with a marker location it was also possible to match measurements from different Optram series. After the matching, the data was reduced to only include measurements for whole metres.

In the second step, the problematic areas were identified by labelling all measurements that exceed set thresholds, a standard deviation of 1 or 2, followed by grouping them into sections of 25 m, 50 m, and 100 m. If one measurement in a section exceeded the thresholds, then the entire section would be labeled as exceeding the thresholds.

In the third step, a function looked through all sections to see if there was any overlap between the Optram measurements that exceeded the thresholds as well as the InSAR measurements that exceeded thresholds. Then the function would classify them into four categories in a confusion matrix (Figure 14). The results from this sensitivity analysis can also be found in Appendix A.

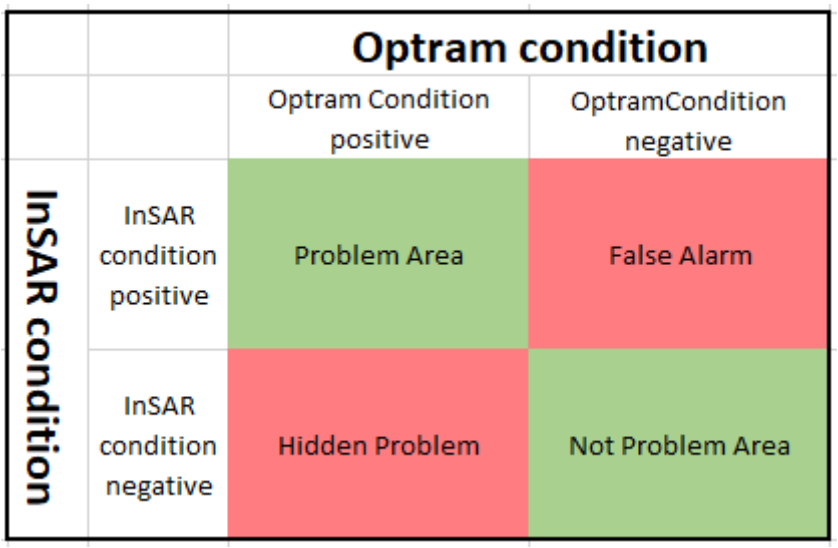

Figure 14. Modified Confusion Matrix. The green squares are areas where Optram and InSAR classification agree. The red squares are for areas were Optram and InSAR classification do not agree

Problem areas refer to sections where both the Optram and InSAR changes exceed the thresholds. The category false alarms are sections where the Optram parameter does not exceed the threshold, but InSAR does. Hidden problems are sections where the Optram changes exceed the thresholds but not the InSAR-derived changes, these are problem sections that InSAR cannot detect. No problem areas are sections where neither the Optram parameter nor the InSAR changes exceed thresholds (Figure 15).

Figure 15. Example of a Classification of InSAR-based and Optram-derived Changes

Lastly, the following three classification measures were computed.

$$\text{Correlation} \qquad \frac{Problem\ Area + Not\ Problem\ Area}{Total\ number\ of\ sections}$$

$$\text{Hidden Rate} \qquad \frac{Hidden\ Problem}{Hidden\ Problem + Problem\ Area}$$

$$\text{False Alarm Rate} \qquad \frac{False\ Alarm}{False\ Alarm + Not\ Problem\ Area}$$

The correlation measures general overlap between Optram and InSAR. Higher correlation means a higher rate of Problem Area and Not Problem Area; in other words, a higher correlation means more agreement between Optram and InSAR. Two other measures were used to see how the classification dealt with Hidden Problems and False Alarms. The Hidden Rate is related to the Hidden Problems, where InSAR is not able to detect problem areas (a false negative), while the False Alarm Rate is related to area where InSAR does detect a problem area, but Optram does not (a false positive).

6.3. Classification Results

Table 6 shows derived classification results for a test where the time range is between December 15 and June 2020 for 50 m long sections and with one standard deviation as the set threshold. Similar tables were generated for the other test settings (Appendix A). Generally, the correlation score was slightly higher for shorter time periods studied, however the false alarm rate was also higher. Generally, the hidden rate was lower for the shorter time periods that were studied. The correlation score was higher in the longer wavelengths for all the studied time periods except for 2016-2017, where shorter wavelengths had a higher correlation. The wavelengths refer to the different section lengths used in the 31 tests.

Table 6. Classification Results for December 2015-June 2020 for 50 m Sections, Under the 1rst Standard Deviation Thresholds

12/2015-6/2020, 50 meter sections, 1st Standard Deviation							
Parameter	Problem Area	False Alarm	Hidden Problem	No Problem	Correlation	HR	FAR
Height Short-wave Left	43	2	147	11	0,27	0,77	0,15
Height Short-wave Right	44	1	147	10	0,27	0,77	0,09
Height Middle-wave Left	28	17	101	57	0,42	0,78	0,23
Height Middle-wave Right	26	19	103	55	0,40	0,80	0,26
Height Long-wave Left	22	23	74	84	0,52	0,77	0,21
Height Long-wave Right	23	22	77	81	0,51	0,77	0,21
Standard deviation Height	22	23	62	96	0,58	0,74	0,19
Standard Deviation Interaction	44	1	158	0	0,22	0,78	1,00

The generally improved performance of the classification with shorter studied time periods may be due to less decorrelation over shorter time periods. The standard deviation for changes in InSAR decreased significantly with shorter time ranges, while it remained almost constant with changes in Optram (Figure 17, Chapter 7.1). This would indicate that the use of smaller standard deviation as thresholds lead to higher correlation.

Although the results from Table 6 might suggest too much variation in the correlation to draw a clear conclusion about the use of InSAR for track condition monitoring, based on the extensive literature review there is a promising future for using InSAR for monitoring railways in combination with other techniques. Although InSAR cannot replace Optram it can be used to complement Optram in finding problem areas in which other techniques can be used to investigate further.

7. Discussion and Conclusions

7.1. Discussion of the Results of Optram and InSAR Comparison

The results from the initial InSAR processing indicate that both subsidence and uplift occur within an 800m wide corridor along the railroad between Kiruna and Riksgränsen. Vertically, the range for the velocities was on average between -10mm/year (subsidence) and +10mm/year (uplift). However, areas around Kirunavaara, Björkliden, and Riksgränsen demonstrated higher subsidence velocities around -25mm/year. The horizontal velocity of displacements was found to be up to 10mm/year in both east and west directions. These results imply that there are certain areas around the railway that experience more vertical and horizontal change than others and that InSAR processing can be used to detect areas where there is more movement. These results are in line with the visual depiction of subsidence along the track as seen in Figure 13 (Chapter 6)

Reducing the studied time period generally increases the performance of the classification. Figure 17 highlights that the standard deviation in mm for changes in InSAR decreases significantly as time period decreases, while remaining almost constant with changes in Optram (Figure 18). This would indicate that the use of a smaller standard deviation as a threshold leads to higher correlation.

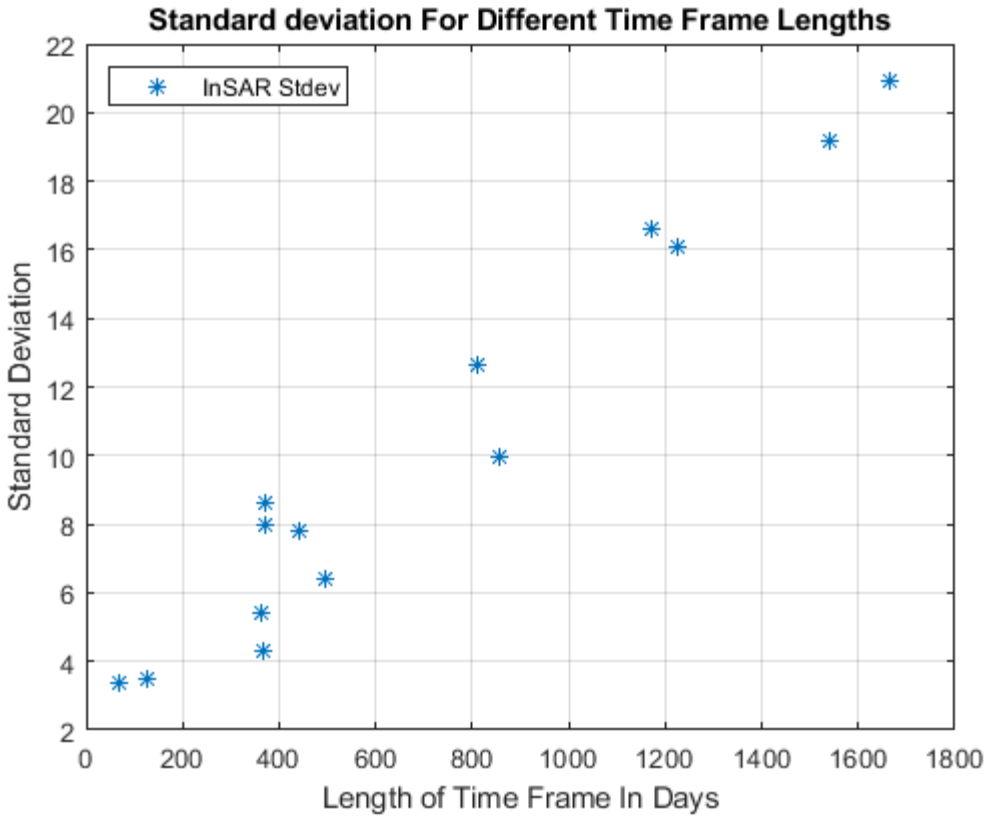

Figure 17. The standard deviation (mm) of displacement increases with longer time periods for InSAR. As the time period increases, changes become more spread (Åmerbilly, 2021)

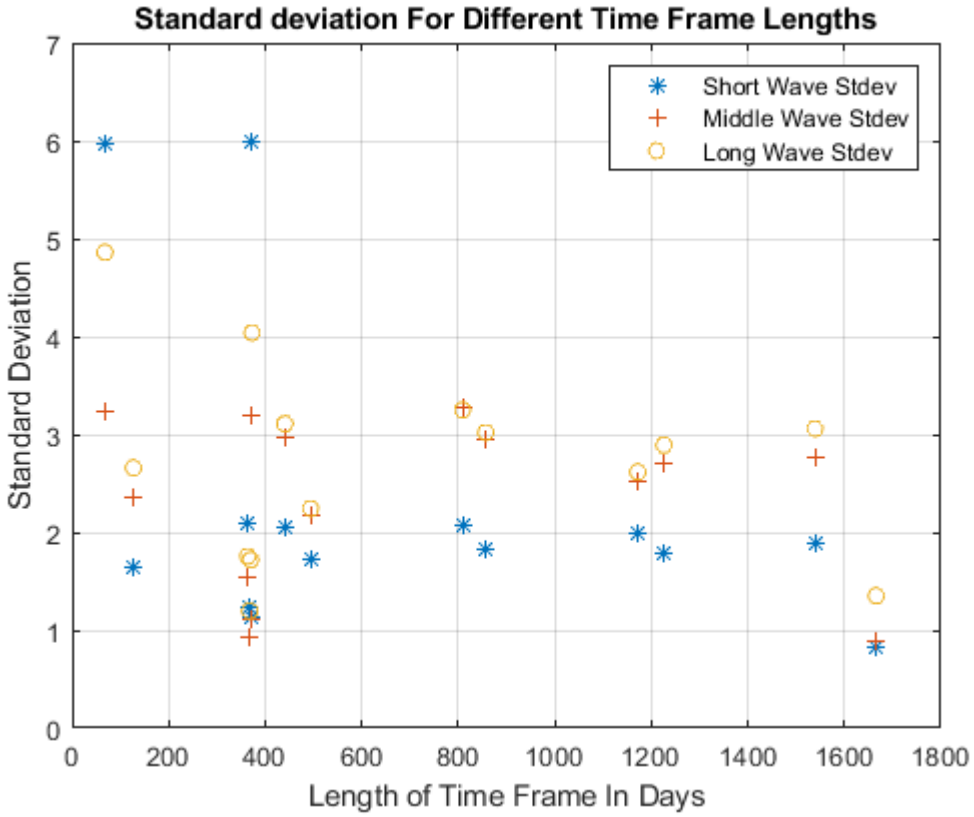

Figure 18. The standard deviation (mm) is almost constant with longer time frames for Optram. Even with longer time periods the spread remains almost the same. Short, medium, and long wave standard deviation refers to the section lengths in m (Åmerbilly, 2021)

In regard to coherence, low coherence can lead to poor deformation detection. The cut-off in for usable points in the classification method was a coherence of 0.5. This meant that almost 92% of all InSAR ground points were removed from the data set, leaving mostly points with coherence between 0.5 and 0.55. The correlation of the remaining points might not be high enough for comparison with a highly accurate and precise monitoring system such as Optram. Other studies have used higher coherence thresholds, such as 0.7 (Bakon, et al., 2016).

Optram and InSAR measure different things and have different spatial and temporal scales. Optram measures the height of the railway with a 25 cm interval, while InSAR measures ground deformation with a 15x15 m cell (Figure 19). This ground cell is affected by scatter from everything inside the cell, not just the rails. This means that the deformation for the rail might be different than for the whole cell. For instance, the track is protected against frost heave, but the surrounding cell is not. Therefore, InSAR cells that include the track are affected by frost heave while the track itself is not.

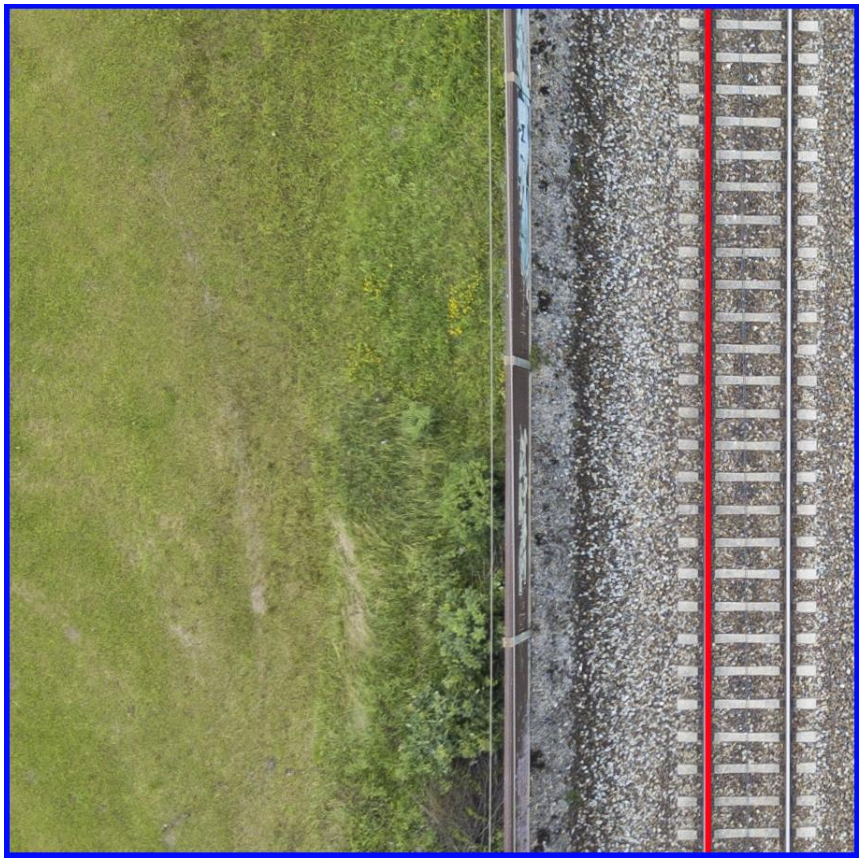

Figure 19. The red line is the rail that Optram measures, while InSAR measures the entire image (Müseler, 2018)

7.2. Conclusions and Future Work

Although Optram and InSAR measure different variables and have different spatial and temporal scales, the two can still be used to complement one another, as Optram measures the track deformation, and InSAR measures the embankment deformation. Additionally, InSAR can be used to detect hotspots in which then other methods such as Optram can be used to further investigate the problem. Similarly, these areas may also need to be investigated further with other in-situ techniques. In general, InSAR can be used as a tool for monitoring the changes occurring on Malmbanan as it can be used for various applications, is cost-efficient, and can be combined with other techniques all depending on the overall goal and objectives of a particular study.

In this study, the ascending and descending geometries results are displayed together. However, in the future some may be interested in investing these separately in order to obtain a better overview of the temporal differences.

Research in the future may revolve around validating with geodetic data, such as precise levelling, or using higher resolution satellites, such as TerraSAR-X. Both would investigate finer spatial resolutions, allowing more investigation of the railway itself as opposed to a large area of land around the railway. A combination of different satellite imagery or imagery from drones may also help with studying a bigger picture, allowing for studying and comparing the different spatial and temporal scales.

The Swedish Ground Motion Survey could be used to investigate ground deformation on a larger scale for all of Sweden. As the survey expands it allow future studies for both private and public sectors to focus on Sweden as a whole but also individual areas around the country.

It will allow for easier access of data across Sweden, which can lead to more studies surrounding ground deformation in various fields including the railway industry.

As mentioned, climate change is expected to play a role in the future degradation of railway tracks globally. InSAR could be used to determine the rate of settlement today caused by a specific weather variable, for example precipitation, which can therefore help determine the rate of change in the future. Modelling of future climate change can be used in combination with results from InSAR processing for determining the impacts of climate change on railways. For instance, due to future climate change, there may be more infrastructural damage on the railways related to track buckling from extreme heat or flooding from extreme amounts of precipitation.

Based on an extensive literature review there is a large potential and a rapidly growing number of applications of InSAR to monitor railways and other types of infrastructure. Additionally, the tools and algorithms for these applications are continuously being improved. The case study, on the other hand, indicated that it can be difficult to directly compare measurement series from different tools, as each works on different resolutions in terms of both time and space. InSAR is thus not about to replace techniques such as those behind Optram. Instead, the approaches offer complementary perspectives, each highlighting different types of issues.

As urban development and climate changes continue it is important to monitor the condition of railways to ensure safe, efficient, and punctual services today and in the future. We find that InSAR offers a good way to identify locations with settlements or other types of ground motions. Especially transition zones between settlements and more stable ground can be challenging from a maintenance point of view and can clearly be identified and monitored using InSAR. With the rollout of national InSAR-data, and the large increase in data accessibility, we see a considerable potential for future studies that apply the technique to the railway area.

References

Ager, T. (2013). An Introduction to Synthetic Aperture Radar Imaging. *Oceanography*, *26*(2), 20-33. 10.5670/oceanog.2013.28

Ahlmer, A-K., Cavalli, M., Hansson, K., Koutsouris, A. J., Crema, S., & Kalantari, Z. (2018). Soil Moisture Remote-Sensing Applications for Identification of Flood-Prone Areas Along Transport Infrastructure. *Environmental Earth Sciences, 77*, 533. http:/10.1007/s12665-018-7704-z. https://www.eionet.europa.eu/etcs/etc-cca/products/etc-cca-reports/tp_3-2013

Aparicio, Á., Leitner, M., Mylne, K., Palin, E., & Sobrino, N. (2013). Support to Transport and Environment Assessments. Adaptation to Climate Change in the Transport Sector. ETC/CCA Technical Paper 03/2013, Bologna, Italy.

Arasteh Khouy, I. (2013). Cost-effective maintenance of railway track geometry: a shift from safety limits to maintenance limits (Doctoral dissertation, Luleå tekniska universitet). http://www.divaportal.org/smash/get/diva2:999211/FULLTEXT01.pdf

Armstrand, T. (2021). *Figure 13. Track Settlement along Malmbanan Track.* Trafikverket.

Arema, L. M. D. (2013). American Railway Engineering and Maintenance-of-Way Association. *Manual for Railway Engineering*.

Asplund, M., Gustafsson, P., Nordmark, T., Rantatalo, M., Palo, M., Famurewa, S. M., & Wandt, K. (2014). Reliability and Measurement Accuracy of a Condition Monitoring System in an Extreme Climate: A Case Study of Automatic Laser Scanning of Wheel Profiles. *Proceedings of the Institution of Mechanical Engineers, Part F: Journal of Rail and Rapid Transit, 228*(6), 695–704. https://doi.org/10.1177/0954409714528485

Avdan, U., & Jovanovska, G. (2016). Algorithm for Automated Mapping of Land Surface Temperature Using LANDSAT 8 Satellite Data. *Journal of Sensors*, *2016*(1480307), 1–8. https://doi.org/10.1155/2016/1480307

Baduge, A.W.A., Henschel, M.D., Hobbs, S., Buehler, S.A., Ekman, J., & Lehrbass, B. (2016). Seasonal Variation of Coherence in SAR Interferograms in Kiruna, Northern Sweden. *International Journal of Remote Sensing*, *37*(8), 370-387. 10.1080/01431161.2014.915435

Baker, C. J., Chapman, L., Quinn, A., & Dobney, K. (2009). Climate Change and the Railway Industry: A review. *Proceedings of the Institution of Mechanical Engineers, Part C: Journal of Mechanical Engineering Science*, *224*(3),519–528. https://doi.org/10.1243/09544062jmes1558

Bergevald, C. (2019). *Using InSAR to Detect Railway Deformations*. (Master's Thesis, Chalmers University of Technology, Gothenburg, Sweden). https://odr.chalmers.se/handle/20.500.12380/300053

Bergquist, B. & Söderholm, P. (2016). Predictive Modelling for Estimation of Railway Track Degradation, edited by Kumar, U. Ahmadi, A., Verma, A.K., Varde, P. in "Current Trends in Reliability, Availability, Maintainability and Safety", Springer International Publishing AG, Cham., 331-347

Bonn, F., & Dixon, R. (2005). Monitoring Flood Extent and Forecasting Excess Runoff Risk with RADARSAT-1 Data. *Natural Hazards, 35*, 377-393. 10.1007/s11069-004-1798-1

Campbell, J., & Wynne, R. (2011). *Introduction to Remote Sensing*, New York: The Guilford Press

Chang, L., Dollevoet, R., & Hanssen, R.F. (2014). Railway Infrastructure Monitoring using Satellite Radar Data. *International Journal of Railway Technology*, *3*(2), 1-14. 10.4203/ijrt.3.2.5

Chang, L., Dollevoet, R. P., & Hanssen, R. F. (2016). Nationwide Railway Monitoring using Satellite SAR Interferometry. *IEEE Journal of Selected Topics in Applied Earth Observations and Remote Sensing*, *10*(2), 596-604. 10.1109/JSTARS.2016.2584783

Chang, L., Sakpal, N. P., Elberink, S. O., & Wang, H. (2020). Railway Infrastructure Classification and Instability Identification using Sentinel-1 SAR and Laser Scanning Data. *Sensors*, *20*(24), 7108. 10.3390/s20247108

Chen, B., Gong, H., Chen, Y., Lei, K., Zhou, C., Si, Y., Li, X., Pan, Y. & Gao, M. (2021). Investigating Land Subsidence and its Causes Along Beijing High-Speed Railway Using Multi-Platform InSAR and a Maximum Entropy Model. *International Journal of Applied Earth Observation and Geoinformation*, *96*, 102284. 10.1016/j.jag.2020.102284

Colesanti, C., & Wasowski, J. (2006). Investigating Landslides with Space-Borne Synthetic Aperture Radar (SAR) Interferometry. *Engineering Geology*, *88*(3–4), 173–199. Retrieved from: https://doi.org/10.1016/j.enggeo.2006.09.013

Crosetto, M., Monserrat, O., Cuevas-González, M., Devanthéry, N., & Crippa, B. (2015). Persistent Scatterer Interferometry: A review. *ISPRS Journal of Photogrammetry and Remote Sensing*, *115*, 78–89. https://doi.org/10.1016/j.isprsjprs.2015.10.011

D'Amico, F., Gagliardi, V., Ciampoli, L. B., & Tosti, F. (2020). Integration of InSAR and GPR Techniques for Monitoring Transition Areas in Railway Bridges. *NDT & E International*, 115, 102291. 10.1016/j.ndteint.2020.102291

Dash, P., Göttsche, F.-M., Olesen, F.-S., & Fischer, H. (2001). Retrieval of Land Surface Temperature and Emissivity from Satellite Data: Physics, Theoretical Limitations and Current Methods. *Journal of the Indian Society of Remote Sensing, 29*(23), 23–30. https://doi.org/10.1007/bf02989910

Deng, H. (2010). Application of Remote Sensing Technique on Investigation of Landslides Along the Li-Xiang Railway. *Second IITA International Conference on Geoscience and Remote Sensing*, *2010*, 363-366. https://doi.org/10.1109/iita-grs.2010.5603073

Ding, P., Jia, C., Di, S., Wu, J., & Wei, R. (2021). Analysis and Evaluation of Land Subsidence along Linear Engineering Based on InSAR Data. *KSCE Journal of Civil Engineering*, *25*(9), 3477-3491. 10.1007/s12205-021-0201-z

Dobney, K., Baker, C.J., Quinn, A.D., & Chapman, L. (2009). Quantifying the Effects of High Summer Temperatures due to Climate Change on Buckling and Rail Related Delays in South-East United Kingdom. *Meteorological Applications, 16*, 245-251. 10.1002/met.114

EN 13848-5. (2008). Railway applications–track–track geometry quality–Part 5: Geometric quality levels. *European Committee for Standardization (CEN)*.

European Commission (2013). *Adapting Infrastructure to Climate Change*. SWD (2013) 137 final of 16/4/2013, Brussels. https://eur-lex.europa.eu/legal-

content/EN/TXT/PDF/?uri=CELEX:52013SC0137&from=EN (Accessed 15 September 2020)

European Commission (2015). *Copernicus Europe's Eyes on Earth.* [Brochure]. European Union. 10.2873/93104 (Accessed 1 September 2020)

European Space Agency (n.d.). *Sentinel-1 User Guide*. https://sentinel.esa.int/web/sentinel/user-guides/sentinel-1-sar (Accessed 1 September 2020)

Ferretti, A., Prati, C., & Rocca, F. (2001). Permanent scatterers in SAR interferometry. *IEEE Transactions on Geoscience and Remote Sensing, 39*(1), 8–20. 10.1109/36.898661

Fryksten, J. (2019). *Study on Ongoing Subsidence in Uppsala City using Sentinel-1 Radar Data.* (Master's Thesis, Gävle University, Sweden). http://www.diva-portal.org/smash/get/diva2:1327631/FULLTEXT03

Fryksten, F., Nilfouroushan, F. (2019). Analysis of Clay-Induced Land Subsidence in Uppsala City Using Sentinel-1 SAR Data and Precise Levelling. *Remote Sensing, 11*(23), 2764. https://doi.org/10.3390/rs11232764

Gabriel, A.K., Goldstein, R.M., & Zebker, H.A. (1989). Mapping Small Elevation Changes Over Large Areas: Differential Radar Interferometry. *Journal of Geophysical Research Solid Earth, 94*(B7), 9183-9191. 10.1029/JB094iB07p09183

Gido N., Bagherbandi M., & Nilfouroushan F. (2020) Localized Subsidence Zones in Gävle City Detected by Sentinel-1 PSI and Leveling Data. *Remote Sensing*, *12*(16), 2629. https://doi.org/10.3390/rs12162629.

Hanssen, R.F. (2002). *Remote Sensing and Digital Image Processing*. Dordrecht: Kluwer Academic Publishers

Hu, F., van Leijen, F.J., Chang, L., Wu, J., and Hanssen, R.F. (2019a). Monitoring Deformation along Railway Systems Combining Multi-Temporal InSAR and LiDAR Data. *Remote Sensing, 11*(19), 2298. https://doi.org/10.3390/rs11192298

Hu, F., Wu, J., Chang, L., & Hanssen, R.F. (2019b). Incorporating Temporary Coherent Scatterers in Multi-Temporal InSAR Using Adaptive Temporal Subsets. *IEEE Transactions on Geoscience and Remote Sensing, 57*(10), 7658-7670. https://doi.org/10.1109/tgrs.2019.2915658

Hooper, A., Segall, P., Zebker, H. (2007). Persistent Scatterer Interferometric Synthetic Aperture Radar for Crustal Deformation Analysis, with Application to Volcán Alcedo, Galápagos. *Journal of Geophysical Research*, *12*, B07407). 10.1029/2006JB004763

IPCC. (2014a). Core Writing Team, Pachauri, R.K. & Meyer, L.A. (eds.) *Climate Change 2014: Synthesis Report. Contribution of Working Groups I, II and III to the Fifth Assessment Report of the Intergovernmental Panel on Climate Change.* IPCC, Geneva, Switzerland. Retrieved from: https://www.ipcc.ch/site/assets/uploads/2018/02/SYR_AR5_FINAL_full.pdf (Accessed 20 November 2020)

IPCC. (2014b). Barros, V.R., Field, C.B., Dokken, D.J., Mastrandrea, M.D., Mach, K.J., Bilir, T.R., Chatterjee, M., Ebi, K.L., Estrada, Y.O., Genova, R.C., Betelhem, G., Kissel, E.S., Levy, A.N., MacCracken, S., Mastrandrea, P.R., & White, L.L. (eds.) *Climate Change 2014: Impacts, Adaptation, and Vulnerability. Part B:*

Regional Aspects. Cambridge University Press, Cambridge, United Kingdom and New York, NY, USA. Retrieved from: https://www.ipcc.ch/site/assets/uploads/2018/02/WGIIAR5-PartB_FINAL.pdf (Accessed 20 November 2020)

Johansson, M., Åkerman, J., Keuper, F., Christensen, T.R., Lantuit, H., & Callaghan, T.V. (2011). Past and Present Permafrost Temperatures in the Abisko Area: Redrilling of Boreholes. *AMBIO*, *40*(6), 558-565. 10.1007/s13280-011-0163-3

Journault, J., Macciotta, R., Hendry, M.T., Charbonneau, F., Huntley, D., Bobrowsky, P.T. (2018). Measuring Displacements of the Thompson River Valley Landslides, South of Ashcroft, BC, Canada, Using Satellite InSAR. *Landslides, 15*, 621–636. https://doi.org/10.1007/s10346-017-0900-1

Kellermann, P., Schöbel, A., Kundela, G., & Thieken, A.H. (2015). Estimating Flood Damage to Railway Infrastructure – The Case Study of the March River Flood in 2006 at the Austrian Northern Railway. *Natural Hazards and Earth System Sciences, 15*, 2485-2496. 10.5194/nhess-15-2485-2015

Kellermann, P., Bubeck, P., Kundela, G., Dosio, A., & Thieken, A.H. (2016). Frequency Analysis of Critical Meteorological Conditions in a Changing Climate - Assessing Future Implications for Railway Transportation in Austria. *Climate, 4*, 25. https://doi.org/10.3390/cli4020025

Kim, S-S., Park, C., Kim, Y-G., Park, C. (2009). Parameter Characteristics of Rail Inspection Measurement System of HSR-350x. *Journal of Mechanical Science and Technology, 23*, 1019-1022. 10.1007/s12206-009-0332-5

Lander, S., & Petersson, J. (2012). *Tamping Planning in Railway Maintenance: Improvement Potential for Optram as Decision Support* (Master's Thesis, Chalmers University of Technology, Gothenburg, Sweden). https://publications.lib.chalmers.se/records/fulltext/159318.pdf

Larsson-Kråik, P.-O. (2012). Managing Avalanches Using Cost–Benefit–Risk Analysis. *Proceedings of the Institution of Mechanical Engineers, Part F: Journal of Rail and Rapid Transit*, 226(6), 641–649. https://doi.org/10.1177/0954409712447168

Li, Z-L., Tang, B-H., Wu, H., Ren, H., Yan, G., Wan, Z., Trigo, I.F., Sobrino, J.A. (2014). Satellite-Derived Land Surface Temperature: Current Status and Perspectives. *Remote Sensing of Environment*, *131*(15), 14-37. https://doi.org/10.1016/j.rse.2012.12.008

Lillesand, T.M., Kiefer, R.W., Chipman, J.W. (2015). *Remote Sensing and Image Interpretation*. Hoboken: John Wiley Sons

Lin, J. (2013). Using Integrated Reliability Analysis to Optimise Maintenance Strategies: A Bayesian Integrated Reliability Analysis of Locomotive Wheels (JVTC Projectnr 274). Division and Maintenance Engineering JVTC – Luleå Railway Research Centre. http://ltu.diva-portal.org/smash/get/diva2:995666/FULLTEXT01.pdf

Lindgren, J., Jonsson, D.K., & Carlsson-Kanyama, A. (2009). Climate Adaptation of Railways: Lessons from Sweden. *EJTIR 9*(2), 164–181. https://journals.open.tudelft.nl/ejtir/article/view/3295/3462

Liu, C., Li, N., Wu, H., & Meng, X. (2014). Detection of High-Speed Railway Subsidence & Geometry Irregularity Using Terrestrial Laser Scanning. *Journal of Surveying Engineering, 140*(3), 1-11. 10.1061/(ASCE)SU.1943-5428.0000131

Luo, Q., Perissin, D., Lin, H., Li, Q., & Duering, R. (2011). Railway Subsidence Monitoring by High Resolution InSAR Time Series Analysis in Tianjin. *IEEE 19th International Conference on Geoinformatics*, pp. 1-4). 10.1109/GeoInformatics.2011.5980745.

Luo, Q., Zhou, G., & Perissin, D. (2017). Monitoring of Subsidence along Jingjin Inter-City Railway with High-Resolution TerraSAR-X MT-InSAR Analysis. *Remote Sensing*, *9*(7), 717. 10.3390/rs9070717

Mattsson, L-G., Jenelius, E. (2015). Vulnerability and Resilience of Transport Systems – A Discussion of Recent Research. *Transportation Research Part A, 81,* 16-34. http://dx.doi.org/10.1016/j.tra.2015.06.002

Meng, X-M., Qi, T-J., Zhao, Y., Dijkstra, T., Shi, W., Luo, Y-F., Wu, Y-Z., Su, X-J., Zhao, F-M., Ma, J-Y., Zhang, Y., Chen, G., Chen, D-X., & Zhang, M-S. (2021) The Deformation of the Zhangjiazhuang High-Speed Railway Tunnel: An Analysis of Causal Mechanisms using Geomorphological Surveys and D-InSAR Monitoring. *Journal of Mountain Science 18*(7), https://doi.org/10.1007/s11629-020-6493-5

Minh, D., Hanssen, R. Rocca, F. (2020). Radar Interferometry: 20 Years of Development in Time Series Techniques and Future Perspectives. *Remote Sensing*, 12(9), 1364. 10.3390/rs12091364

Misnevs, B., Melikyan, A., & Bazaras, D. (2015). Hazard Assessment of Weather Factors for the Occurrence of an Emergency on the Railway. *Procedia Computer Science, 77,* 40–47. https://doi.org/10.1016/j.procs.2015.12.357

Moreira, A., Prats-Iraola, P., Younis, M., Krieger, G., Hajnsek, I., & Papathanassiou, K. P. (2013). A Tutorial on Synthetic Aperture Radar. *IEEE Geoscience and Remote Sensing Magazine*, *1*(1), 6-43. 10.1109/MGRS.2013.2248301

NASA (8, October 2020). *Landsat Science.* NASA. https://landsat.gsfc.nasa.gov/ (Accessed 8 October 2020)

Nolte, R., Kamburow, C., & Rupp, J. (2011). *UIC Project ARISCC Adaptation of Railway Infrastructure to Climate Change Final Report (6th draft version).* Berlin. https://trimis.ec.europa.eu/sites/default/files/project/documents/20150811_132352_32476_Adaptation_of_Railway_Infrastructure.pdf (Accessed 5 October 2020)

Nordmark, T., & Larsson-Kråik, P-O. (2007). Managing rail degradation on the Malambanan. *Railway Gazette International 163*(6), 369-372. https://www.railwaygazette.com/in-depth/managing-rail-degradation-on-the-malmbanan/25039.article

Pawluszek-Filipiak, K., Borkowski, A. (2020). Integration of DInSAR and SBAS Techniques to Determine Mining-Related Deformations Using Sentinel-1 Data: The Case Study of Rydułtowy Mine in Poland. *Remote Sensing*, *12*(2), 242. 10.3390/rs12020242

Poreh, D., Iodice, A., Riccio, D., & Ruello, G. (2016). Railways' Stability Observed in Campania (Italy) by InSAR Data. *European Journal of Remote Sensing*, 49(1), 417-431. 10.5721/EuJRS20164923

Qin, X., Liao, M., Zhang, L., & Yang, M. (2017). Structural Health and Stability Assessment of High-Speed Railways via Thermal Dilation Mapping with Time-Series InSAR Analysis. *IEEE Journal of Selected Topics in Applied Earth Observations and Remote Sensing*, 10(6), 2999-3010. 10.1109/JSTARS.2017.2719025

Samiei-Esfahany, S. (2017). *Exploitation of Distributed Scatterers in Synthetic Aperture Radar Interferometry*. (Doctoral dissertation, Delft University of Technology, Delft, Netherlands). 10.4233/uuid:22d46f1e-9061-46b0-9726-760c41404b6f

Schaefer, K., Liu, L., Parsekian, A., Jafarov, E., Chen, A., Zhang, T., Gusmeroli, A., Panda, S., Zebker, H.A., & Schaefer, T. (2015). Remotely Sensed Active Layer Thickness (ReSALT) at Barrow, Alaska Using Interferometric Synthetic Aperture Radar. *Remote Sensing, 7*(4), 3735-3759. https://doi.org/10.3390/rs70403735

Serrano-Juan, A., Pujades, E., Vázquez-Suñè., E., Crosetto, M., & Cuevas-González, M. (2017). Levelling vs. InSAR in Urban Underground Construction Monitoring: Pros and Cons. Case of la Sagrera Railway Station (Barcelona Spain). *Engineering Geology, 218*(2017), 1-11. http://dx.doi.org/10.1016/j.enggeo.2016.12.016

Singhroy, V., Li, J., & Charbonneau, F. (2015). High Resolution Rapid Revisit InSAR Monitoring of Surface Deformation. *Canadian Journal of Remote Sensing*, *41*(5), 458-472. 10.1080/07038992.2015.1104638

Soleimanmeigouni, I. (2019). *Predictive Models for Railway Track Geometry Degradation* (Doctoral dissertation, Luleå University of Technology, Luleå. Sweden). http://www.diva-portal.org/smash/get/diva2:1286681/FULLTEXT01.pdf

Soleimanmeigouni, I., Ahmadi, A., Nissen, A., & Xiao, Z. (2020). Prediction of Railway Track Geometry Defects: A Case Study. *Structure and Infrastructure Engineering, 16*(7), 987- 1001. 10.1080/15732479.2019.1679193

Sol-Sánchez, M., & D'Angelo, G. (2017). Review of the Design and Maintenance Technologies used to Decelerate the Deterioration of Ballasted Railway Tracks. *Construction and Building Materials, 157*(30), 402-415. http://dx.doi.org/10.1016/j.conbuildmat.2017.09.007

Sveriges Geologiska Undersökning *Kartgenerator.* Sveriges Geologiska Undersökning. http://apps.sgu.se/kartgenerator/maporder_sv.html (Accessed 10 October 2021)

Tosti, F., Gagliardi, V., D'Amico, F., & Alani, A.M. (2020). Transport Infrastructure Monitoring by Data Fusion of GPR and SAR Imagery Information. *Transportation Research Procedia, 45*(2020), 771-778. https://doi.org/10.1016/j.trpro.2020.02.097

Trafikverket (2018). *Optram Användarmanual*. Trafikverket https://www.trafikverket.se/contentassets/872ff542f5cf429a8b330098424622ee/optram_anvandarmanual.pdf (Accessed 24 May 2021)

Trafikverket (2020a). *Presentation of system Optram*. Trafikverket. https://www.trafikverket.se/contentassets/872ff542f5cf429a8b330098424622ee/presentation-av-optram-200318.pdf (Accessed 24 May 2021)

Trafikverket (2020b). *Datadokumentation och inställningsfiler i Optram.* Trafikverket. https://mobil.trafikverket.se/contentassets/872ff542f5cf429a8b330098424622ee/200227-datadokumentation-och-installningsfiler-i-optram.pdf (Accessed 24 May 2021)

Trafikverket (2021a). *Optram*. Trafikverket. https://www.trafikverket.se/optram (Accessed 30 September 2021)

Trafikverket (2021b). *Malmbanan*. Trafikverket. https://www.tra_kverket.se/nara-dig/Norrbotten/vibygger- och-forbattrar/Malmbanan/ (Accessed 30 September 2021)

Wasowski, J., & Bovenga, F. (2014). Investigating Landslides and Unstable Slopes with Satellite Multi Temporal Interferometry: Current Issues and Future Perspectives. *Engineering Geology*, *174*, 103–138. https://doi.org/10.1016/j.enggeo.2014.03.003

Wempen. J.M., & McCarter, M.K. (2017). Comparison of L-band and X-band Differential Interferometric Synthetic Aperture Radar for Mine Subsidence Monitoring in Central Utah. *International Journal of Mining Science and Technology, 27*(1), 159-163. https://doi.org/10.1016/j.ijmst.2016.11.012

Xu, P., Liu, R. K., Wang, F., Wang, F. T., & Sun, Q. X. (2013). Railroad Track Deterioration Characteristics Based Track Measurement Data Mining. *Mathematical Problems in Engineering*, *2013*. http://dx.doi.org/10.1155/2013/970573

Yang, Z. (2015). *Monitoring and Predicting Railway Subsidence Using InSAR and Time Series Prediction Techniques.* (Doctoral dissertation, The University of Birmingham, UK). https://etheses.bham.ac.uk/id/eprint/6377/1/Yang15PhD.pdf

Yang, Z., Schmid, F., & Roberts, C. (2015). Assessment of Railway Performance by Monitoring Land Subsidence. *6th IET Conference on Railway Condition Monitoring.* 10.1049/cp.2014.1000

Yhokha, A., Goswami, P.K., Chang, CP., Yen, JY., Ching, KE., Aruche, K.M. (2018). Application of Persistent Scatterer Interferometry (PSI) in Monitoring Slope Movements in Nainital, Uttarakhand Lesser Himalaya, *Journal of Earth System Science*, *127*(6), 10.1007/s12040-017-0907-y

Zhang, B., Wdowinski, S., Oliver-Cabrera, T., Koirala, R., Jo, M.J., & Osmanoglu, B. (2018). Mapping the Extent and Magnitude of Server Flooding Induced by Hurricane Irma with Multi-Temporal Sentinel-1 SAR and InSAR Observations. *International Archives of the Photogrammetry, Remote Sensing and Spatial Information Sciences, XLII*(3), 2237-2244. https://doi.org/10.5194/isprs-archives-XLII-3-2237-2018

Zhang, Q., Li, Y., Zhang, J., & Luo, Y. (2019). InSAR technique applied to monitoring of the Qinghai-Tibet Railway. *Natural Hazards and Earth Systems Sciences 19*(10), 2229-2240. https://doi.org/10.5194/nhess-19-2229-2019

Zhang, Z., Wang, M., Liu, X., Wang, C., Zhang, H., Tang, Y., & Zhang, B. (2019). Deformation Feature Analysis of Qinghai–Tibet Railway Using TerraSAR-X and Sentinel-1A Time-Series Interferometry. *IEEE Journal of Selected Topics in Applied Earth Observations and Remote Sensing*, *12*(12), 5199–5212. https://doi.org/10.1109/jstars.2019.2954104

Zhao, R., Li, Z-W., Feng, G-C., Wang, Q-J., & Hu, J. (2016). Monitoring surface deformation over permafrost with an improved SBAS-InSAR algorithm: With emphasis on climatic factors modeling. *Remote Sensing of Environment, 184*, 276-287. https://doi.org/10.1016/j.rse.2016.07.019

Zhou, H., Wang, Y., Yan, S., Li, Y., Liu, X., & Zhang, F. (2018). Monitoring of Recent Ground Surface Subsidence in the Cangzhou Region by the Use of the InSAR Time-Series Technique with Multi-Orbit Sentinel-1 TOPS imagery*. International Journal of Remote Sensing, 39*(22), 8113-8128. 10.1080/01431161.2018.1482020

Åmerbilly, K. (2021). *Interferometric Synthetic Aperture Radar for Track Condition Monitoring: Case Study on Malmbanan.* (Master's Thesis, Lund University, Lund, Sweden). https://lup.lub.lu.se/luur/download?func=downloadFile&recordOId=9065042&fileOId=9065046